THE ASTROPHYSICAL JOURNAL SUPPLEMENT SERIES, 55:585–595, 1984 August

H I SHELLS, SUPERSHELLS, SHELL-LIKE OBJECTS, AND "WORMS"

CARL HEILES
Astronomy Department, University of California, Berkeley
Received 1983 August 31; accepted 1984 February 15

ABSTRACT

We present photographic representations of the combination of two H I surveys, so as to eliminate the survey boundaries at $|b| = 10°$. We also present high-contrast photographs for particular velocities to exhibit weak H I features. All of these photographs were used to prepare a new list of H I shells, supershells, and shell-like objects. We discuss the structure of three shell-like objects that are associated with high-velocity gas, and with gas at all velocities that is associated with radio continuum loops I, II, and III. We use spatial filtering to find wiggly gas filaments—"worms"—crawling away from the galactic plane in the inner Galaxy. The "worms" are probably parts of shells that are open at the top; such shells should be good sources of hot gas for the galactic halo.

We review the observational data on shells and supershells. There is no unique relationship between shells and any other type of astronomical object. Stellar winds and supernovae in stellar associations are adequate energy sources for many shells. However, they are inadequate for the largest observed supershells unless star-formation activity is much greater than usual. Furthermore, they do not easily account for the properties of some of the unusual shell-like objects. An alternative energy source, the collision of high-velocity clouds with the galactic disk, is consistent with several aspects of the data.

Subject headings: nebulae: general — nebulae: supernova remnants — radio sources: 21 cm radiation

I. INTRODUCTION

Photographic representations of the angular structure of H I in small velocity intervals reveal a multitude of filamentary structure. Many of these filaments are curved arcs that appear to be portions of small circles on the sky. In some cases the sizes of these arcs change with velocity. Such arcs are expected from stationary or expanding shells.

Heiles (1979; hereafter Paper I) has presented a list of shells and "supershells" in the galactic plane, i.e., below 10° in latitude. More shells are visible in the photographic representations of H I by Colomb, Pöppel, and Heiles (1980), which covered the sky above latitude 10°. In these papers, the boundaries of $|b| = 10°$ arise because of the different surveys used; the former paper used the galactic plane survey of Weaver and Williams (1973), while the latter used the surveys of Heiles and Habing (1974) and of Colomb *et al.*

Casual perusal of the H I photographs indicates that many H I structures cross the boundaries $|b| = 10°$. The present paper combines the two sets of survey data to produce photographic representations that continuously cover the latitude range $-65°$ to $+65°$. These photographs, together with the resulting list of shells and supershells, are presented in § II. Some of these objects may not really be shells, but instead may be shell-like objects that have some of the observational characteristics of true shells. Section III discusses some individual objects that are of particular interest and also presents some additional photographs at higher contrast in selected velocity ranges. Section IV presents the results of crude experiments with spatial filtering of data at $|b| < 10°$, which show the presence of incomplete shells—"worms"—in the inner galaxy. Section V reviews the existing observational data and the theoretical interpretation, and § VI summarizes the paper.

II. OBSERVATIONAL DATA AND A NEW LIST OF SHELLS, SUPERSHELLS, AND SHELL-LIKE OBJECTS

The observational data for this section consist of two 21 cm line surveys, those of Weaver and Williams (1973), which covers $|b| < 10°$, and of Heiles and Habing (1974), which covers the higher latitudes. Both surveys were taken with the same equipment, and both zero levels and intensity scales are defined very accurately. The H I profiles were integrated over small velocity ranges and projected onto rectangular projections in galactic longitude and latitude. Photographic representations of these projections are presented in Figure 1 (Plates 10–18). The longitude range covered is that of the Weaver and Williams survey, 10° to 250°, and the velocity range covered is -89.7 to 38.0 km s^{-1} in increments of 6.3 km s^{-1} at velocities more negative than -45 and 8.4 km s^{-1} at velocities more positive than -40 km s^{-1}. These photographs severely undersample the survey data in velocity, which have velocity resolution 2 km s^{-1}.

These photographs reveal a great deal of structure, most of which is filamentary. One gains the impression that many of the filaments form portions of closed circles. Detailed examination reveals that, in some cases, filaments change position with velocity, in the manner expected for expanding spherical shells. We assume that all such filaments are portions of shells.

Table 1 presents a catalog of shells derived from our examination of these photographs. In this list, we have not included shells that are in the previous compilation of Paper I,

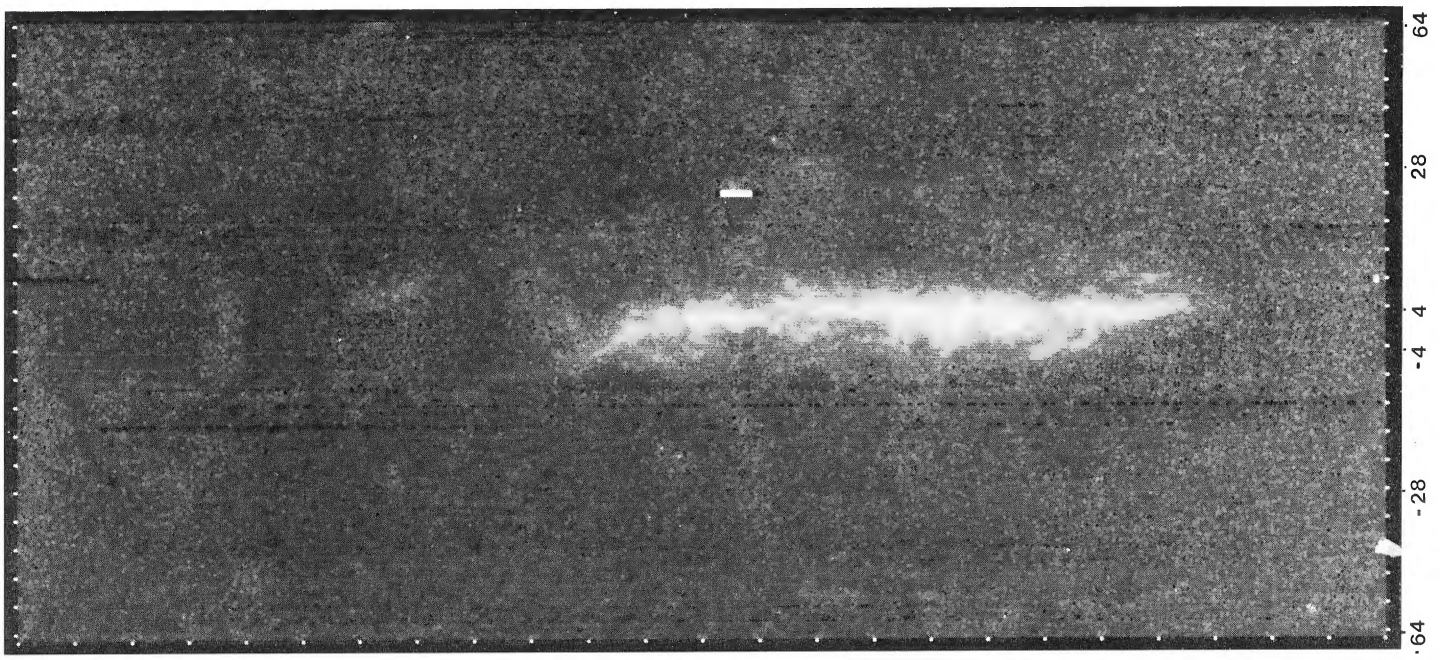

FIG. 1*b*.—Same as Fig. 1*a*, but centered at LSR velocity -83.4 km s^{-1}

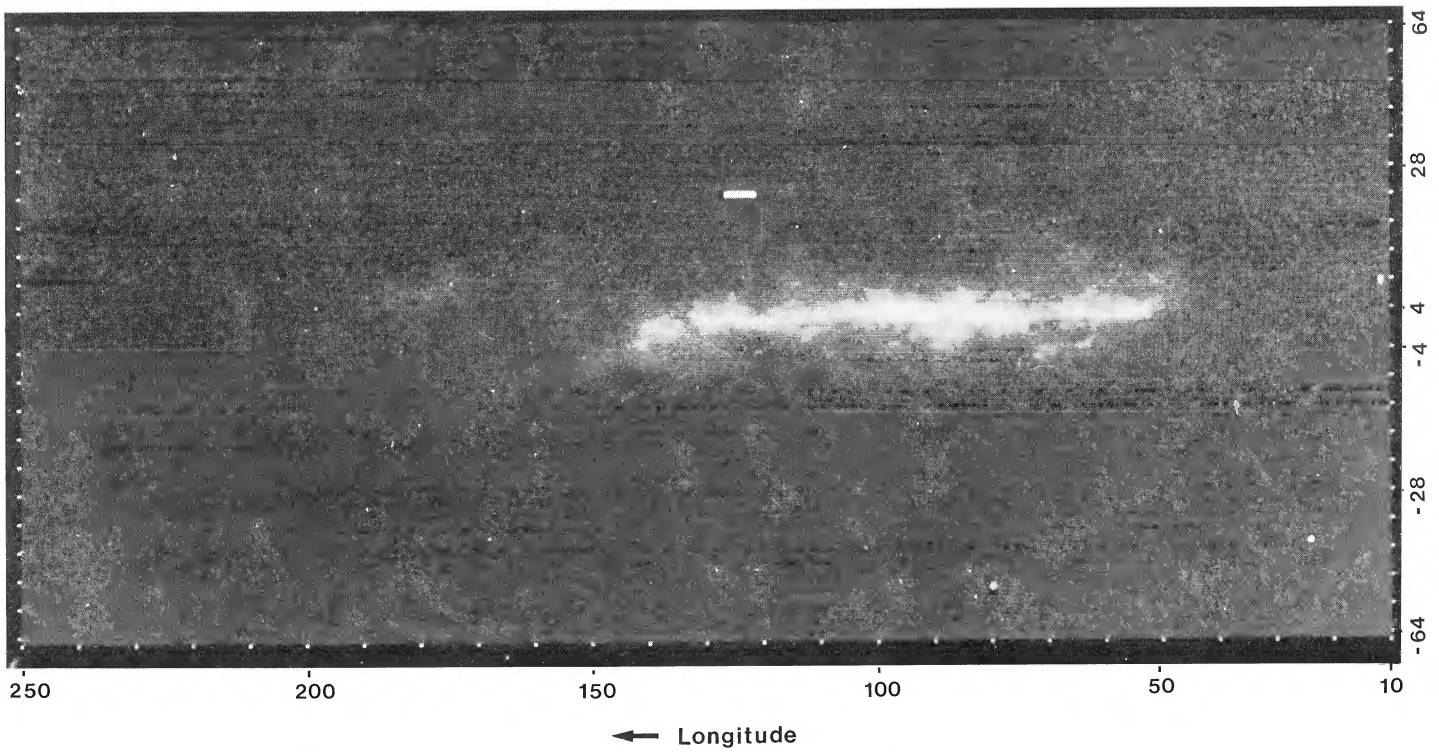

FIG. 1*a*.—Photographic representation of H I column density centered at LSR velocity -89.7 km s^{-1}; areas with larger column densities are whiter. Longitude increases from 10° at the right to 250° at the left, with tick marks every 10°. Latitude increases to 65° at the top and decreases to $-65°$ at the bottom, with tick marks at $|b| = 4°$, 10°, 16°,...,52°, 58°, 64°.

HEILES (*see* page 585)

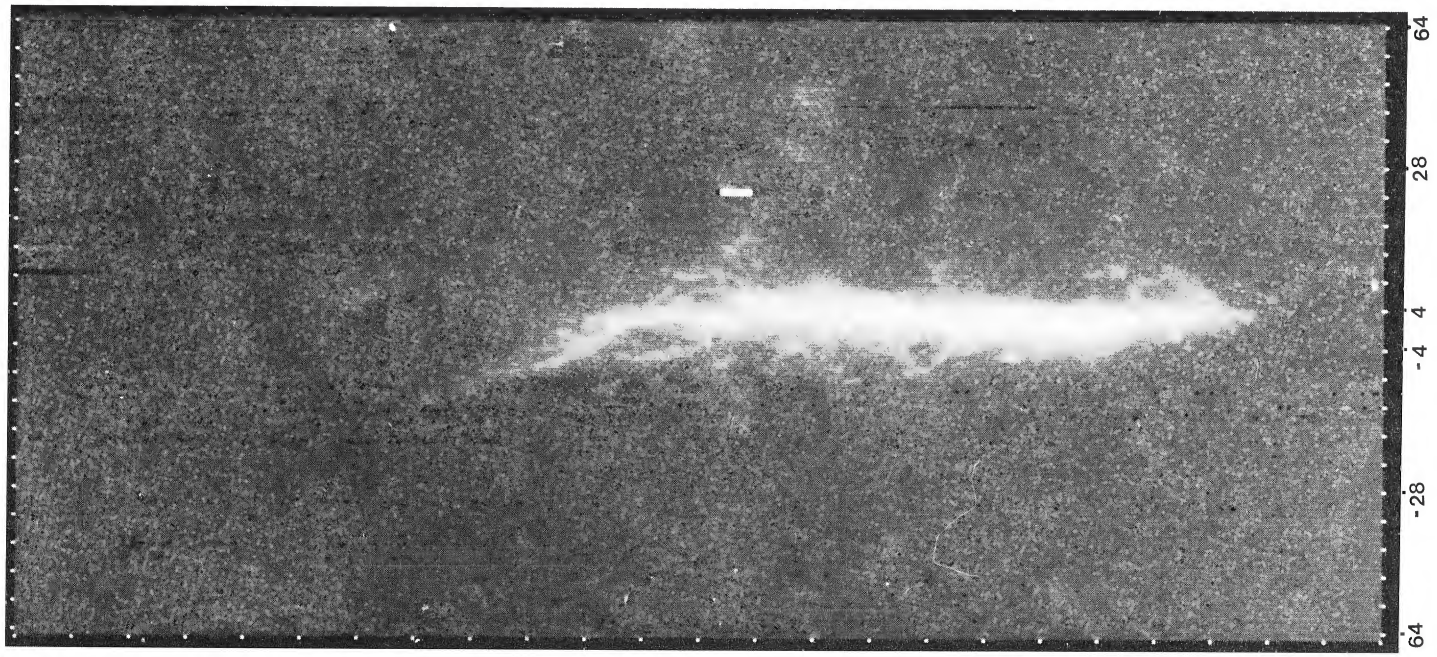

FIG. 1*d*.—Same as Fig. 1*a*, but centered at LSR velocity -70.7 km s^{-1}

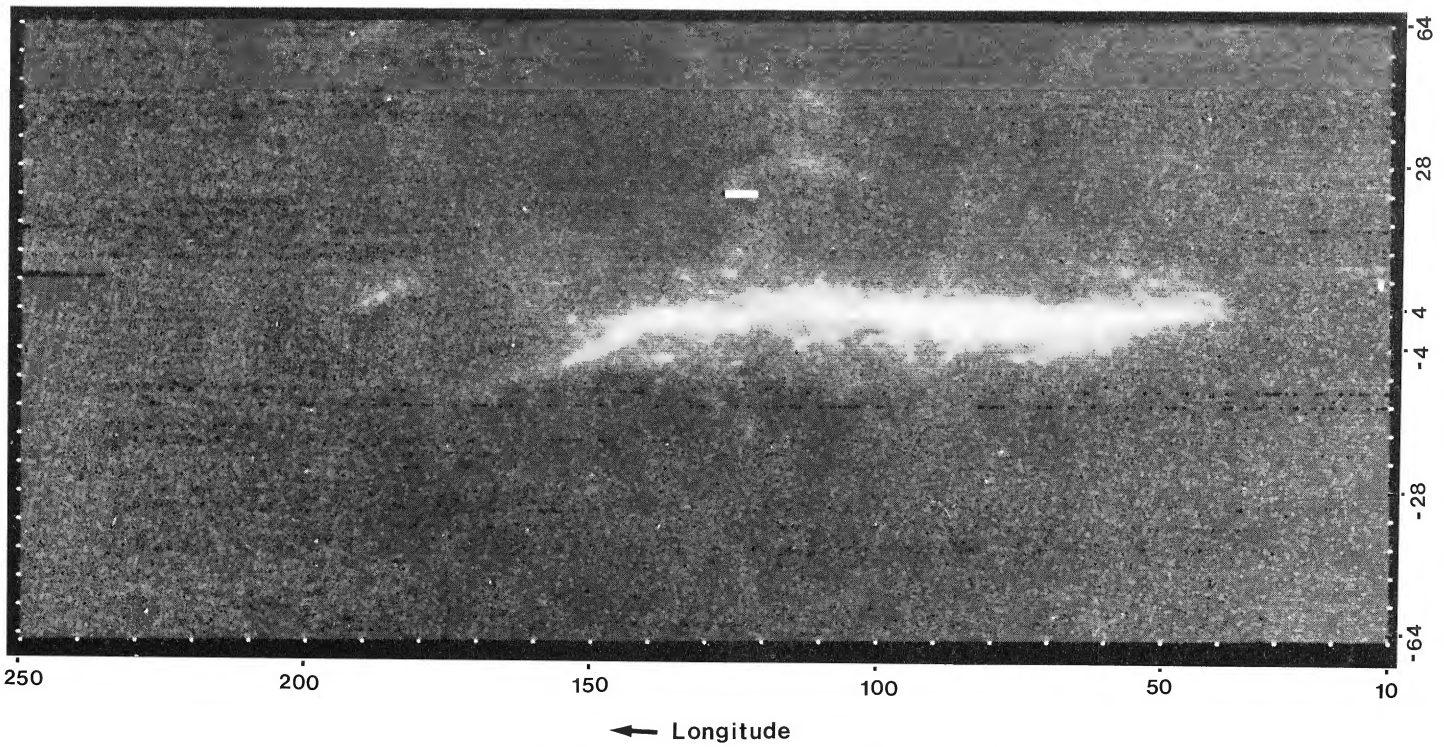

FIG. 1*c*.—Same as Fig. 1*a*, but centered at LSR velocity -77.1 km s^{-1}

HEILES (*see* page 585)

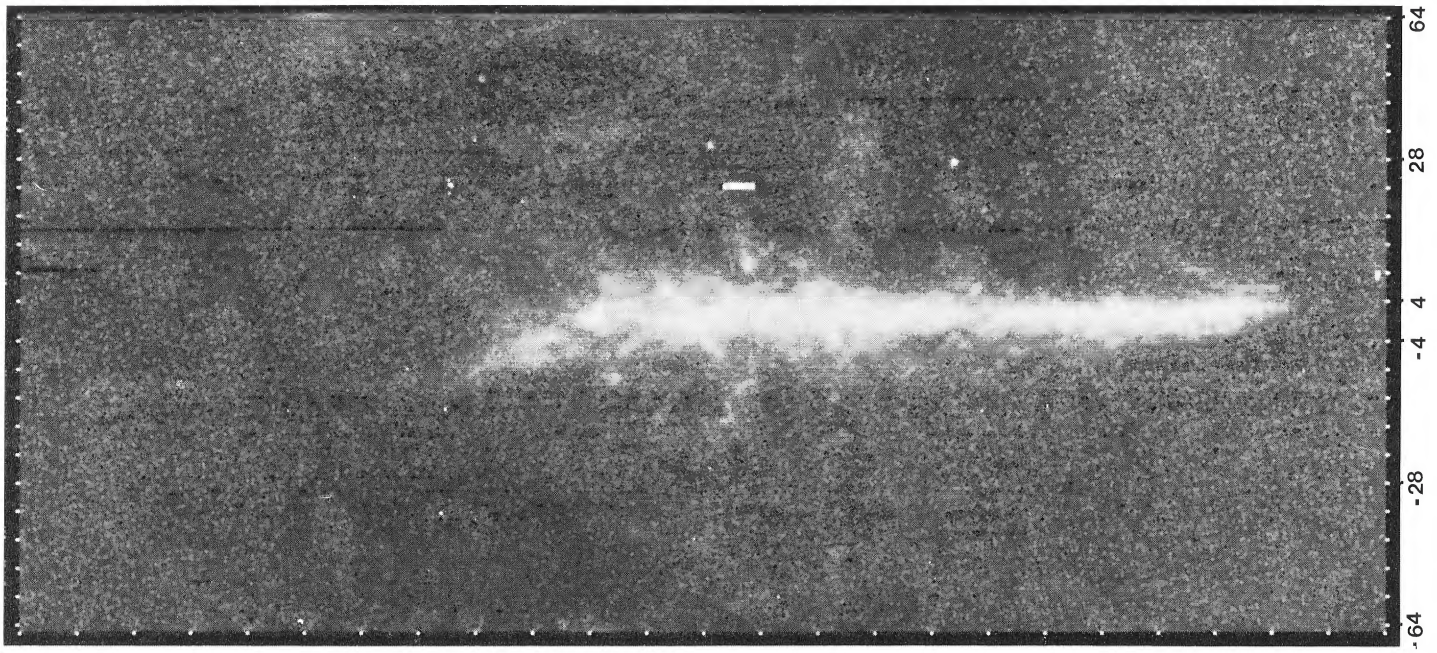

FIG. 1*f*.—Same as Fig. 1*a*, but centered at LSR velocity −58.1 km s^{-1}

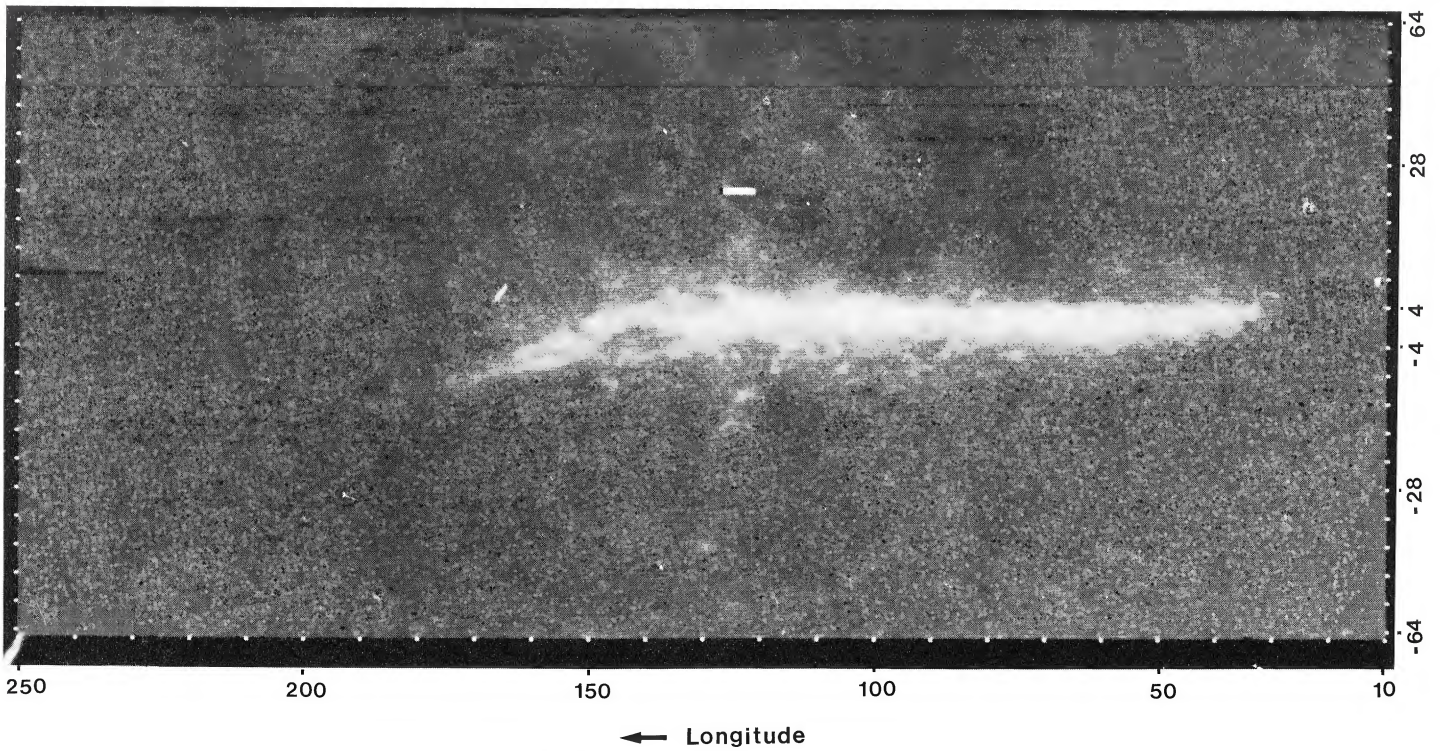

FIG. 1*e*.—Same as Fig. 1*a*, but centered at LSR velocity −64.4 km s^{-1}

HEILES (*see* page 585)

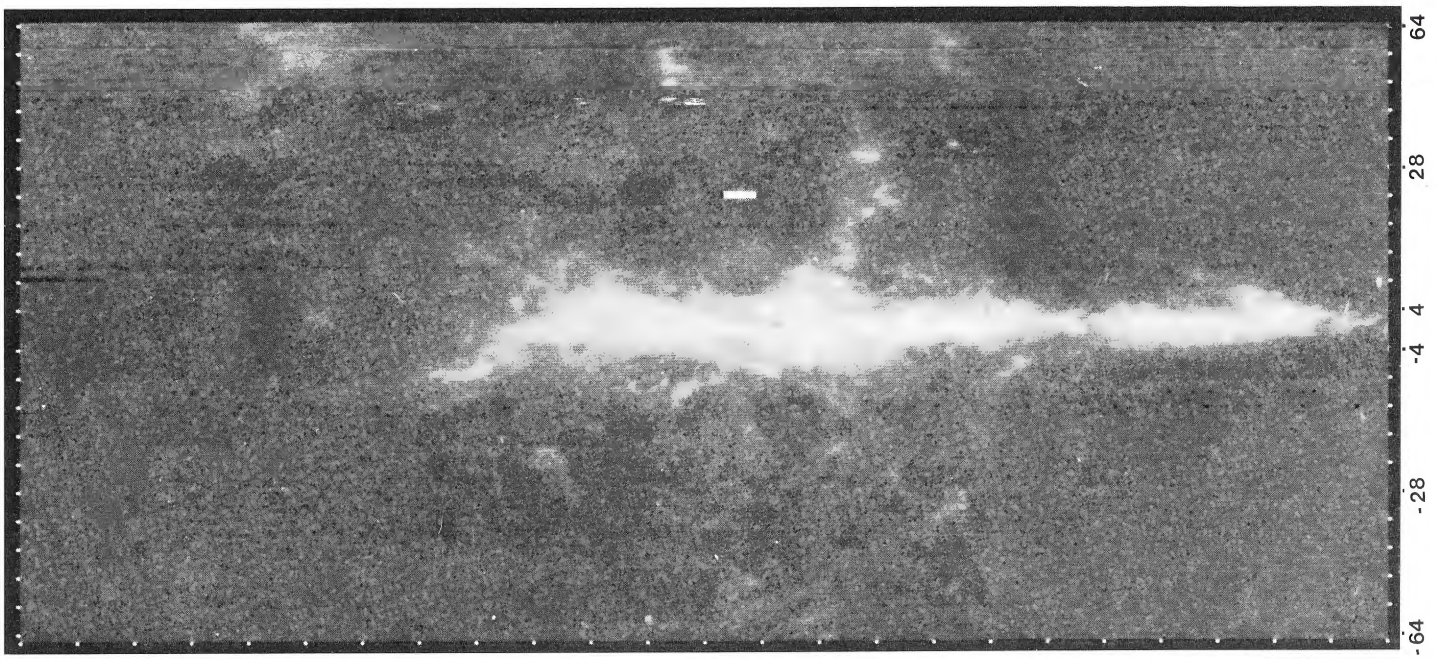

FIG. 1*h*.—Same as Fig. 1*a*, but centered at LSR velocity -45.4 km s^{-1}

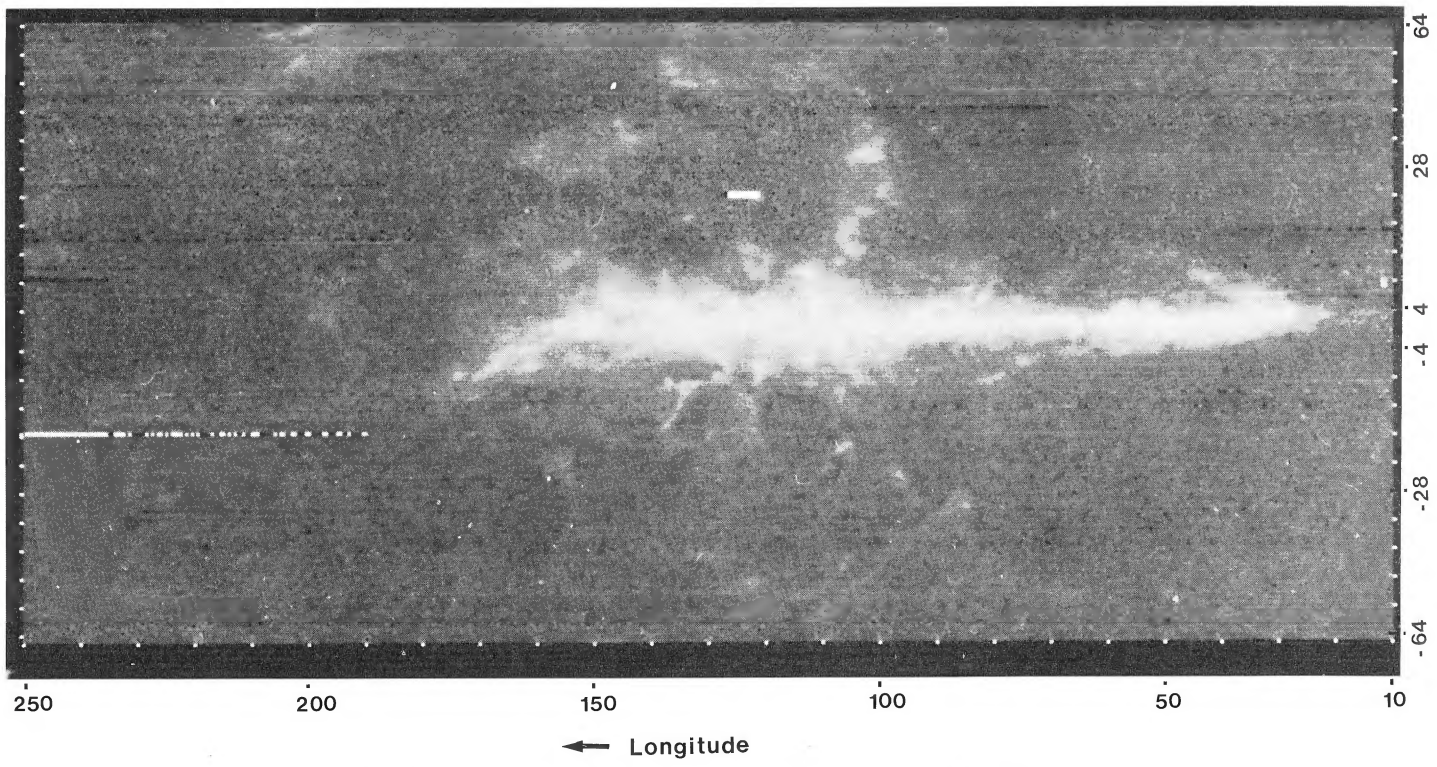

FIG. 1*g*.—Same as Fig. 1*a*, but centered at LSR velocity -51.8 km s^{-1}

HEILES (*see* page 585)

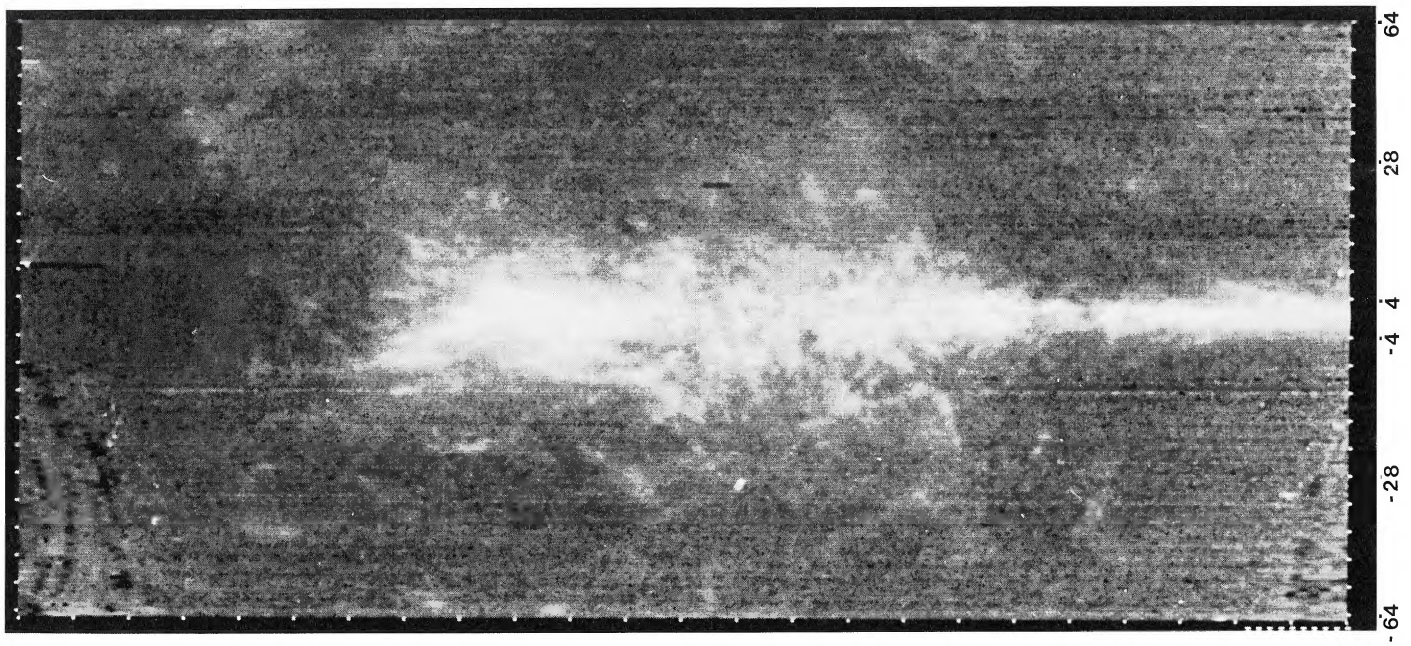

FIG. 1*j*.—Same as Fig. 1*a*, but centered at LSR velocity −29.6 km s^{-1}

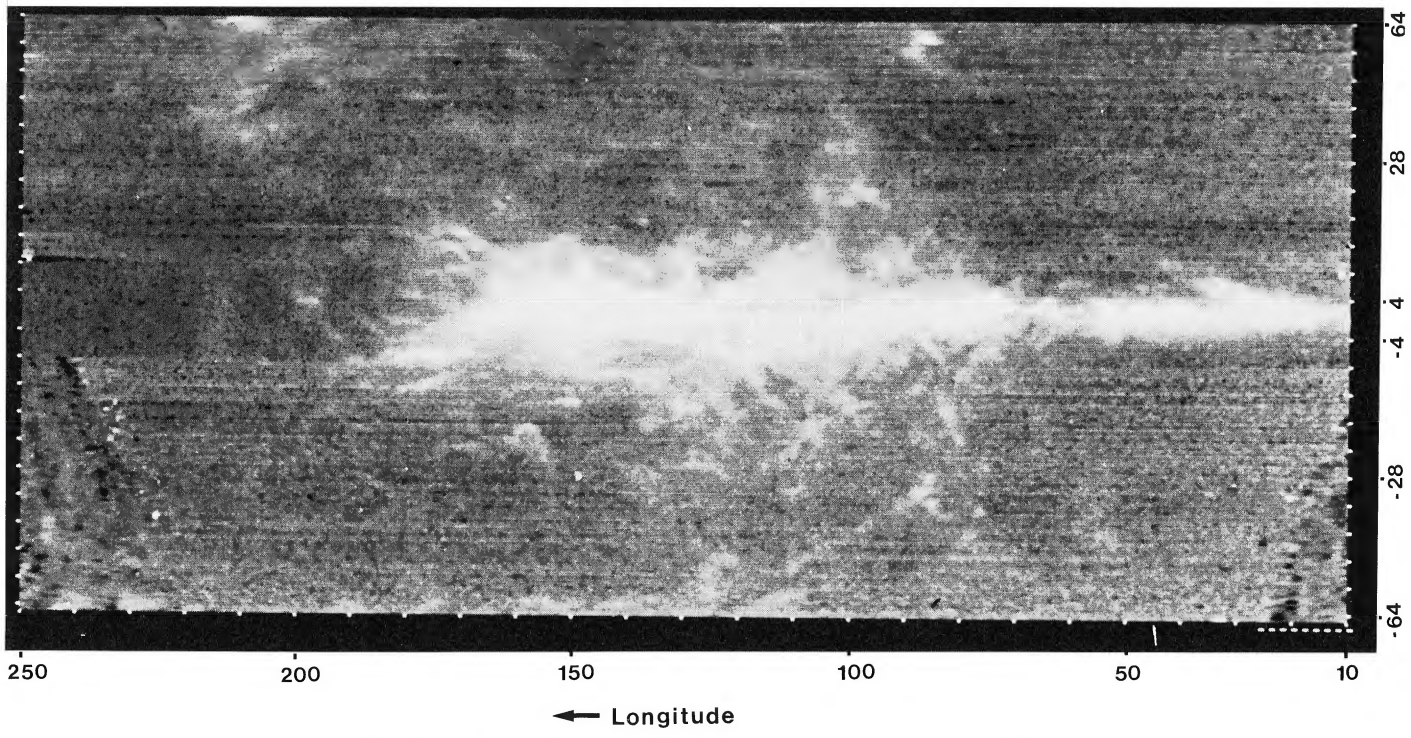

FIG. 1*i*.—Same as Fig. 1*a*, but centered at LSR velocity −38.0 km s^{-1}

HEILES (*see* page 585)

PLATE 15

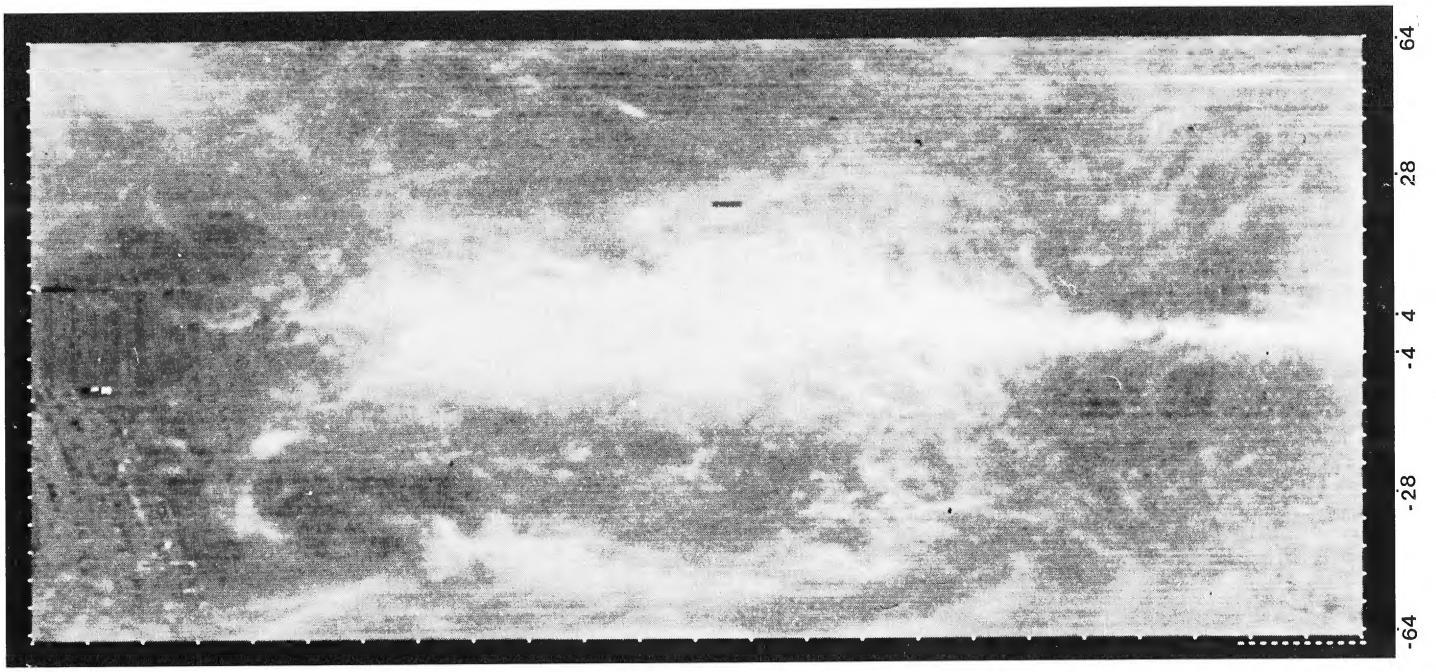

FIG. 1*l*.—Same as Fig. 1*a*, but centered at LSR velocity -12.7 km s^{-1}

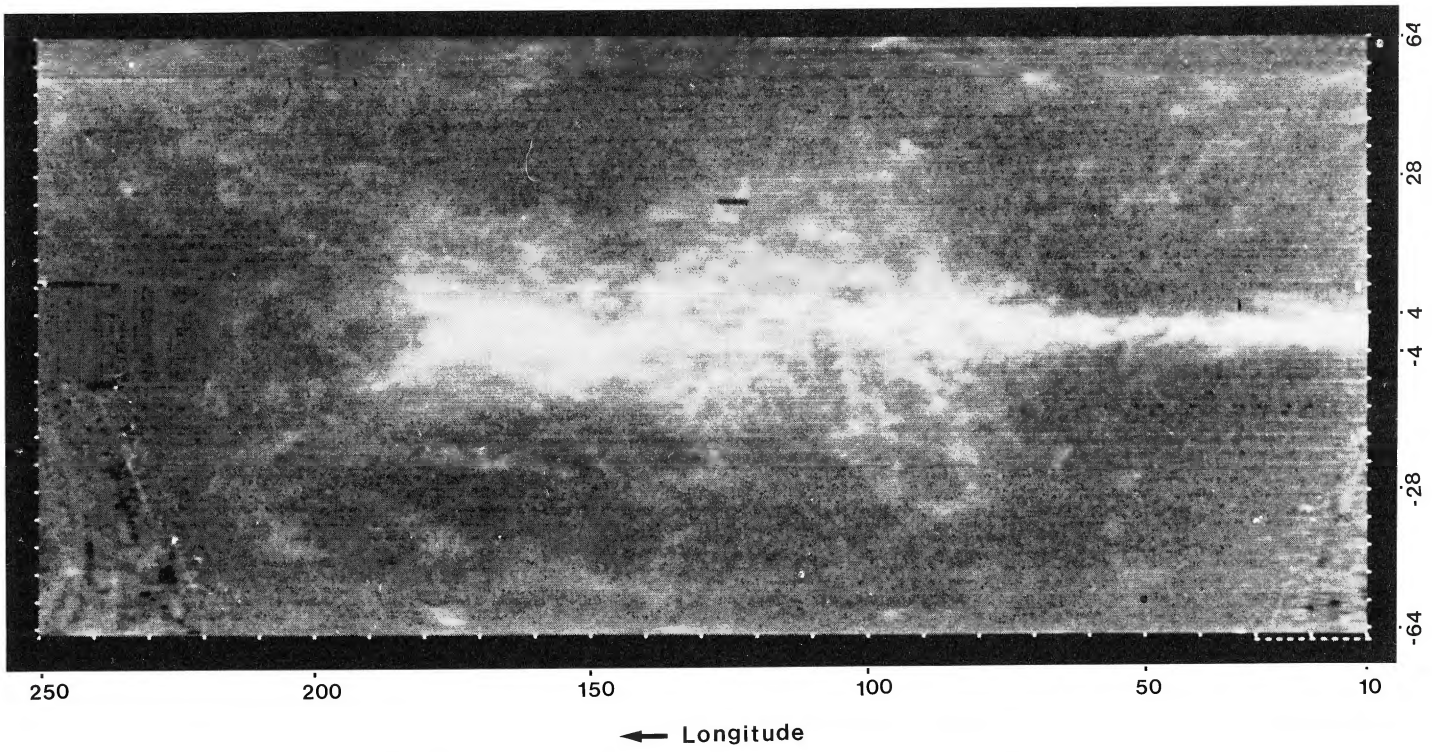

FIG. 1*k*.—Same as Fig. 1*a*, but centered at LSR velocity -21.6 km s^{-1}

HEILES (*see* page 585)

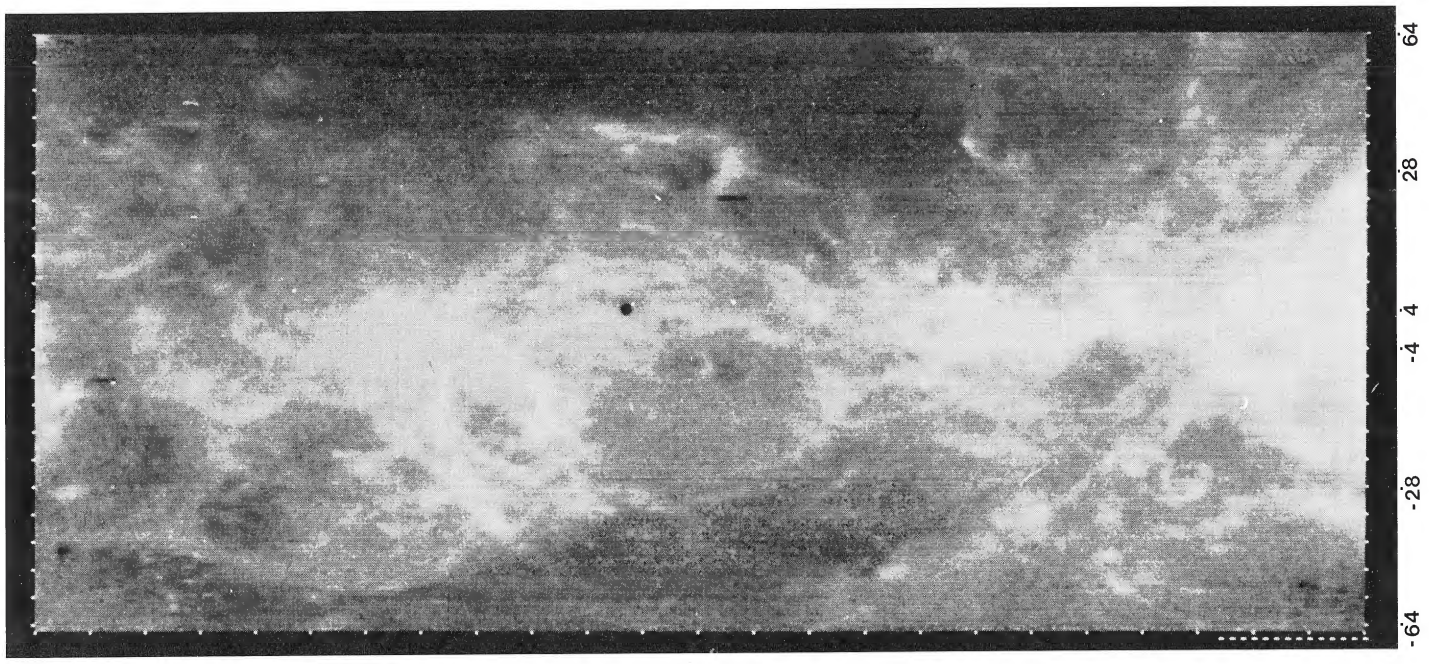

FIG. 1*n*.—Same as Fig. 1*a*, but centered at LSR velocity +4.2 km s^{-1}

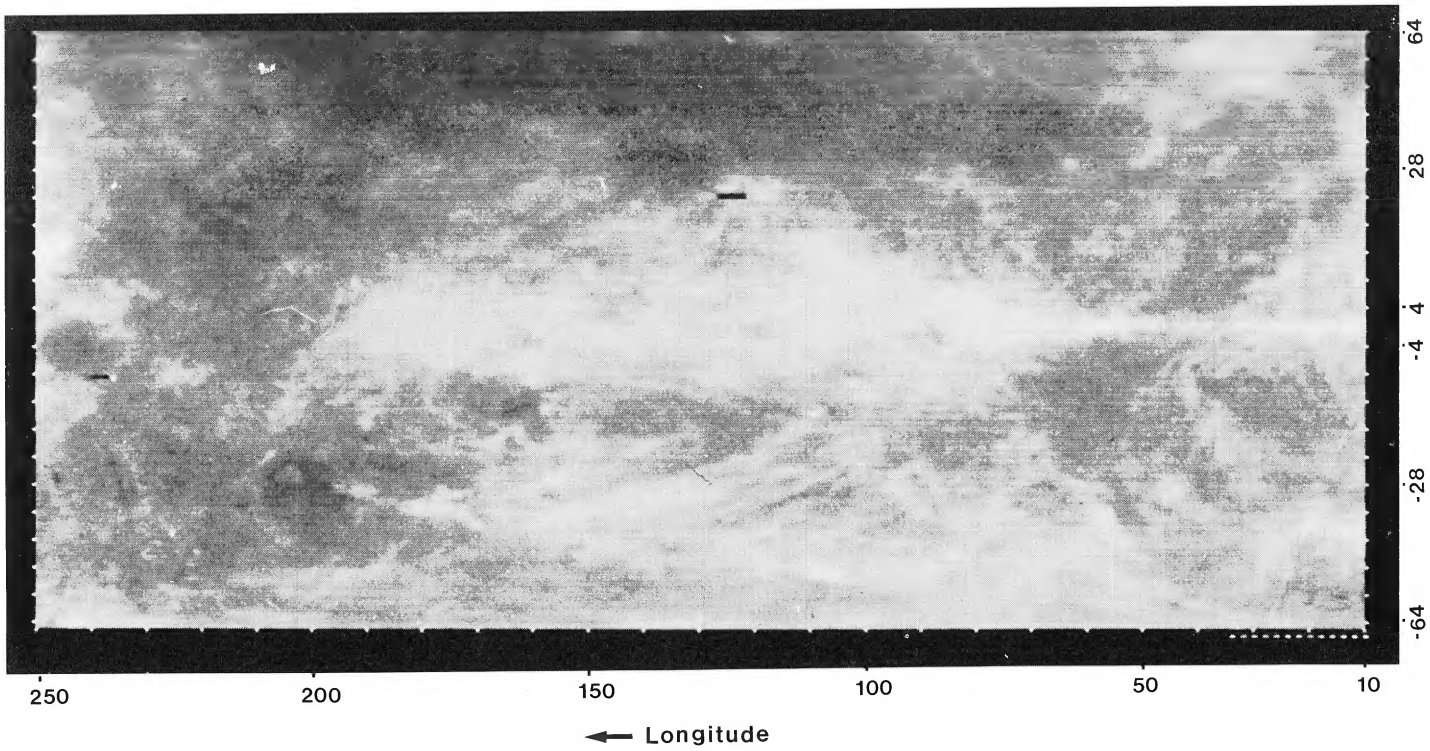

FIG. 1*m*.—Same as Fig. 1*a*, but centered at LSR velocity −4.2 km s^{-1}

HEILES (*see* page 585)

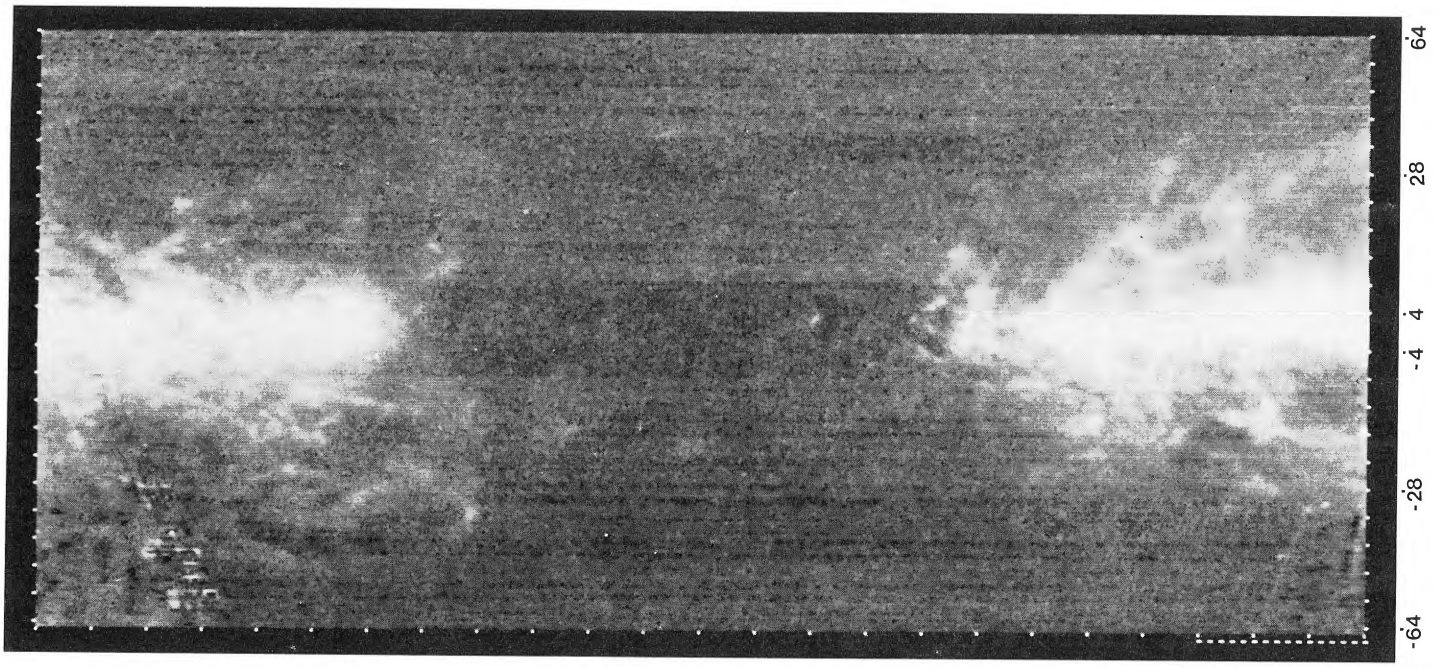

FIG. 1*p*.—Same as Fig. 1*a*, but centered at LSR velocity +21.1 km s^{-1}

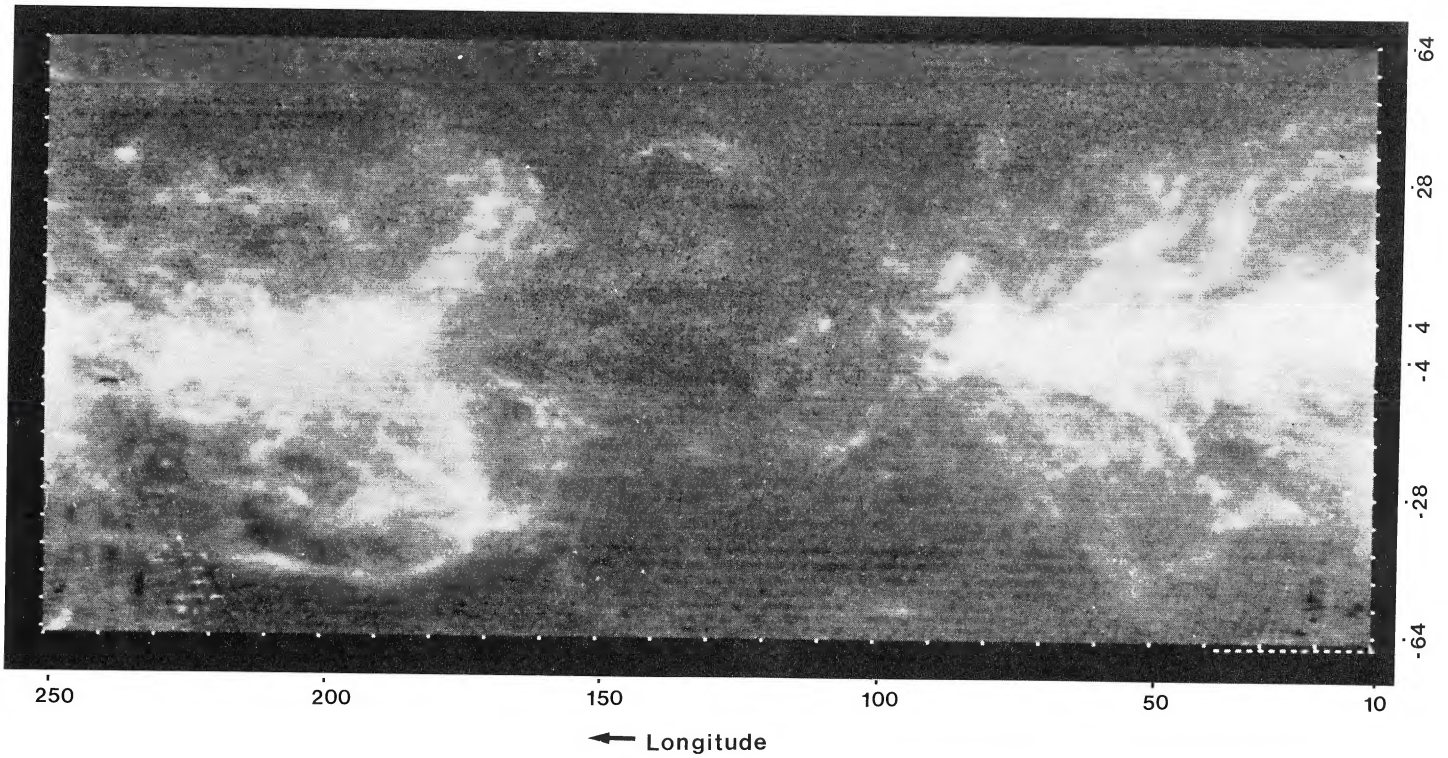

FIG. 1*o*.—Same as Fig. 1*a*, but centered at LSR velocity +12.7 km s^{-1}

HEILES (*see* page 585)

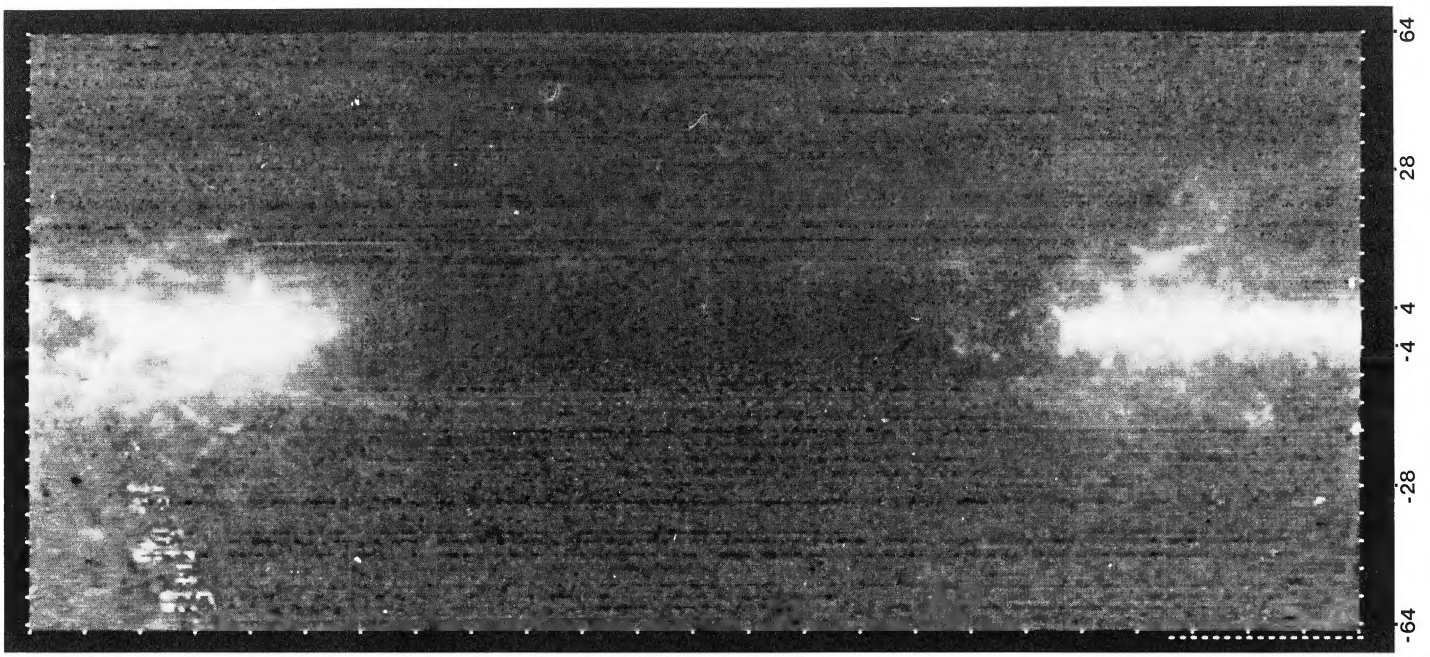

FIG. 1*r*.—Same as Fig. 1*a*, but centered at LSR velocity +38.0 km s^{-1}

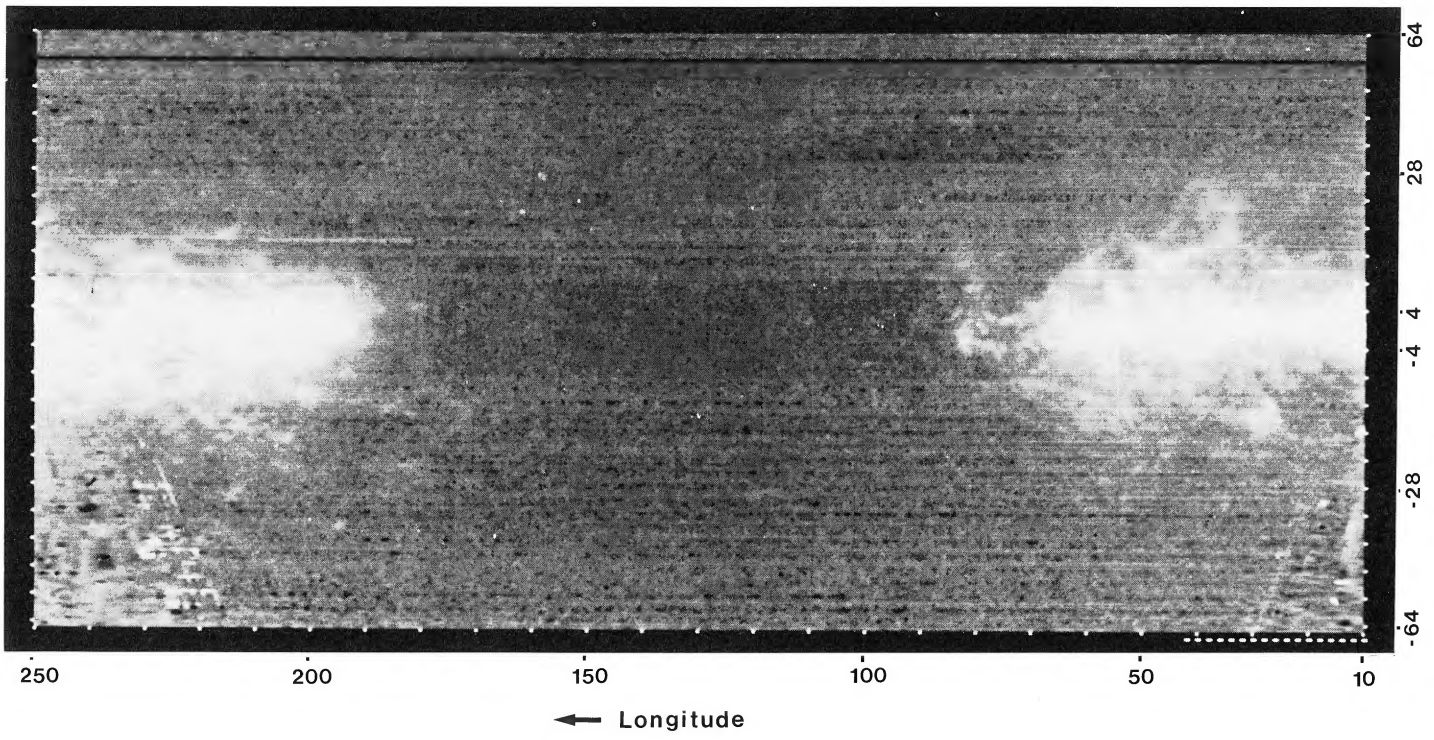

FIG. 1*q*.—Same as Fig. 1*a*, but centered at LSR velocity +29.6 km s^{-1}

HEILES (*see* page 585)

TABLE 1

H I SHELLS AND SHELL-LIKE OBJECTS

Name (1)	Δl (deg) (2)	Δb (deg) (3)	V_{min} (km s^{-1}) (4)	V_{max} (km s^{-1}) (5)	R_{gal} (kpc) (6)	Distance (kpc) (7)	Diameter (l) (pc) (8)	Diameter (b) (pc) (9)
GS 017−14+13[a]	25	20	4.2	21.1	8.3	17.2/1.4	591	489
GS 032+26+8	24	25	4.2	4.2	9.4	16.2/0.7	270	314
GS 045+20+13	14	13	12.7	21.1	9.4	13.3/0.9	206	204
GS 054+12+25	10	14	21.1	29.6	8.8	9.5/2.3	384	550
GS 058+08−71	10	7	−77.1	−64.4	16.4	19.6	3368	2394
GS 067+44+4[b]	28	20	−4.2	12.7	9.8	7.4/0.5	161	160
GS 078+15−84	15	15	−90	−77.1	15.2	13.8	3488	1806
GS 081−07−49	12	8	−51.8	−45.4	12.5	9.2	1912	1285
GS 088+11−64	3	6	−70.7	−58.1	13.5	9.4	482	984
GS 088+18−4	31	28	−4.2	−4.2	10.163	2.2	1131	1075
GS 90−28−17	18	21	−21.6	−12.7	10.7	3.8	1053	1392
GS 90−04−8	10	9	−4.2	−12.7	10.2	2.0	349	314
GS 91+12−80	4	4	−83.4	−77.1	14.8	10.7	727	651
GS 94+18−17	8	11	−21.6	−12.7	10.8	3.4	445	643
GS 102+18−41	12	19	−51.8	−29.6	12.0	5.2	1026	1708
GS 104+08−26	9	8	−29.6	−21.6	11.2	3.2	497	447
GS 107−12−13	10	6	−12.7	−12.7	10.6	1.6	272	168
GS 109+22−17	44	24	−21.6	−12.7	10.8	2.0	1387	817
GS 113+18−22	15	8	−21.6	−21.6	11.1	2.3	572	321
GS 114−08−64	8	7	−70.7	−58.1	14.2	6.8	881	771
GS 115−19−52	18	24	−45.4	−58.1	13.0	5.1	1514	2136
GS 120−30−8	110	50?	−13	−4	...	...	...	...
GS 124+10−61	9	8	−83.4	−37.9	14.2	5.9	911	823
GS 125−10−58	6	8	−64.4	−51.8	14.0	5.6	577	781
GS 127+30−52	57	45	−58.1	−45.4	...	...	...	...
GS 130−38−50	100	70	−70.7	−29.6	...	...	...	...
GS 131−19+4	41	37	4.2	4.2	...	...	...	...
GS 135+08−34	11	6	−38.0	−29.6	12.4	3.1	589	324
GS 135+29+4	30	27	−4.2	12.7	...	...	...	...
GS 136−09−44	18	6	−58.1	−29.6	13.4	4.3	1329	450
GS 137−27−17	17	17	−21.6	−12.7	11.3	1.5	383	430
GS 144+10−41	7	6	−45.4	−38.0	14.0	4.6	553	482
GS 152+12−51	6	7	−64.4	−38.0	17.7	8.2	840	1001
GS 155+38−58	105	65	−70.7	−45.4	...	...	...	...
GS 165−21−4	23	13	−21.6	4.2	10.7	0.72	269	163
GS 174+02−64	38	28	−89.7	−38.0	...	...	...	...
GS 193−32+4	55	43	−12.7	21.1	10.8	0.82	800	615
GS 202−28+12	19	16	4.2	21.1	11.5	1.6	467	446
GS 216−17+38	14	8	38.0	38.0	13.5	4.1	957	572
GS 226−09+30	9	9	21.1	38.0	12.0	2.7	410	439
GS 243−16+25	8	7	21.1	29.6	11.3	2.3	308	281
GS 331+14−15	120	90	−34	4	...	...	...	...

[a] Low-longitude end extends beyond edge of maps in Fig. 1.
[b] Irregular shape change with velocity.

which used only the Weaver and Williams survey data and is thus restricted to $|b| < 10°$. Thus, Table 1 contains only those shells that cross $|b| = 10°$ or that are located entirely outside $|b| = 10°$.

Table 1 suffers because we did not use modern image processing techniques. Instead, we used hard copy photographs and gray-scale images to detect shells. This prevented us from using spatial filtering and variable contrast to facilitate the recognition of structure. Furthermore, it prevented us from making accurate estimates of column density. This is the reason that no information is presented concerning column density, mass, or energy.

Many of the entries in Table 1 are uncertain because recognition of a shell is a subjective process. In some cases filaments appear at only one velocity, that is on only one photograph; in others, the filaments change position from one photograph to the next, and there are so many filaments that intersections are common. Thus, it is often difficult to tell whether a filament is really an individual structure, whether it is formed by an agglomeration of other filaments, and whether it should be associated with one that is located at a slightly different position on another photograph. Furthermore, many filaments are not closed circles. Not only does this add to the uncertainty in shell parameters, but it renders uncertain the entire assumption that all filaments are portions of shells. Finally, there is a selection effect against shells of small angular diameter. This occurs for two reasons. The first is the 0°.5 angular resolution of the H I surveys. The second is the large angular area covered by the photographs, which has biased our subjective eye toward large shells.

In summary, Table 1 is entirely unsuitable for statistical purposes. The entries in Table 1 are based on a subjective judgement of the above confusing factors. We believe that each entry represents a real structural entity. However, some entries probably represent structures other than shells. Others probably represent more than one real shell, and some shells are probably represented by more than one entry. Undoubtedly the large majority of shells is not represented in Table 1 at all. A specific illustration of the statistical biases induced by the methods used to recognize shells is the comparison of Hu's (1981) list with ours; nearly all of her shells have diameters smaller than 10°, while most of ours are larger than 10°.

Column (1) contains the shell name, which specifies the approximate longitude, latitude, and LSR velocity of the shell center, as in Paper I. Columns (2) and (3) contain the shell diameter in longitude and latitude, respectively. Columns (4) and (5) contain the approximate minimum and maximum LSR velocities at which the shell is visible on the photographs. Column (6) contains the galactocentric radius of the shell, calculated assuming that the Sun is 10 kpc from the galactic center and that the galaxy has a flat rotation curve with rotation velocity 250 km s^{-1}. Column (7) contains the distance of the shell from the Sun, and columns (8) and (9) contain the linear diameter of the shell in the directions of longitude and latitude, respectively.

The distances quoted in Table 1 are kinematic distances. Kinematic distances are reliable only for objects that have fairly large velocities and that are located away from longitude 180°. For shells, one might suspect that kinematic distances are less reliable than usual because the shells might have a larger component of random velocity than average. However, this possible extra random velocity cannot be very important. If it were, many shells would have "forbidden" velocities, in contrast to the observed situation. While a few shells do have slightly forbidden velocities, they are of the amounts that can be ascribed to the ordinary random motions of the interstellar gas. In fact, in the modern observational and theoretical (e.g., McKee and Ostriker 1977) picture of the intersteller medium, the random motions of the interstellar gas arise mainly from expansion of shells, so that the random motion of shells is, by definition, equal to the average random motion. Finally, for an expanding shell, the expansion motion can be separated from galactic rotation by the change in shell diameter with velocity. A few shells have velocities that are anomalies; these are discussed below.

Shells located inside the solar circle have two possible distances from the Sun. Both of these distances are given in Table 1, but the linear diameters in Table 1 are derived on the assumption that the shells are located at the nearer distance.

The uncertainties about the individual entries in Table 1 imply that the derivation of detailed information about individual objects is overinterpretation, particularly without using image processing techniques. For statistical purposes, a very approximate estimate of the mass swept up by a shell is 8.5 $R_{sh}^2 M_\odot$, where R_{sh} is the shell radius in parsecs. This is a fit to the shells of Paper I and assumes that all shells have the same H I column density. This assumption is usually correct to within a factor of 3 or so, but is certainly incorrect for easily recognized shells that have unusually large column densities.

III. DISCUSSION OF SOME INDIVIDUAL OBJECTS

a) GS 120−30−8

This shell, which is visible on Figures 1*l*, 1*m*, and 1*n*, overlaps with radio continuum loop II and is comparable in size— $\sim 110° \times 50°$ in l and b. This shell is even clearer on the photographs of Colomb, Pöppel, and Heiles (1980), which have the advantage of better velocity sampling. From these pictures one gains the impression that the H I filaments decrease in diameter from −8 to +4 km s^{-1}, in the manner expected for an expanding shell. If it is an expanding shell, then we are seeing the receding portion of the shell at the more positive velocities.

This shell lies next to a filament having higher negative velocity gas—the classical "intermediate-velocity" (IV) gas (see review by Verschuur 1975). Some of this gas is dimly visible on Figures 1*d*–1*j*. Higher contrast photographs, which include only this $|b| > 10$ data, are given in Figure 2 (Plates 19–22); Figures 2*b*–2*d* show the IV gas more clearly. The IV gas consists of a very thin, arc-shaped filament running from $(l, b) \approx (85, -35)$ to $(150, -60)$, between velocities of −71 to −46 km s^{-1}; it is barely discernible at the higher negative velocities.

Near $(l, b) = (140, -55)$, a high-velocity (HV) filament centered at −110 km s^{-1} begins and runs to about $(180, -45)$ (Cohen 1981). This HV filament follows the H I emission at −13 km s^{-1} almost exactly.

Figure 3 summarizes the locations of the HV, IV, and low-velocity H I filaments, together with radio continuum loop II. The apparent superposition of gas at widely differing velocities is not consistent with the simple model of an expanding shell, unless the different velocities correspond to the approaching and receding hemispheres. In this case, one might interpret Cohen's HV gas and the low-velocity gas as being the approaching and receding hemisphere of the same shell; the IV gas, which lies outside both the HV and low-velocity filaments, would define the outer periphery and full size of the shell. This shell would have a net systemic velocity of about −50 km s^{-1}.

Alternatively, Cohen (1981) argues that this is not a true shell but is instead what we are calling a shell-like object. In his picture, the H I in this region is the result of the collision of infalling HV gas with ambient gas. The −10 km s^{-1} filament has been accelerated from 0 to −10 km s^{-1} by the shock produced by the collision; the −110 km s^{-1} gas is the shocked, cooled gas that was originally infalling. A difficulty with Cohen's picture is the fact that the HV filament covers only a fraction of the length of the low-velocity filament, and there is no large difference between the properties of the low-velocity filament where it is superposed with HV gas and where it is not. This difficulty might be only apparent if the HV gas is neutral, and thus detectable as H I, over only part of its length. Optical and UV lines sometimes reveal the presence of HV ionized gas associated with nearby H I at the same velocity, particularly at negative latitudes (Heiles 1974). The magnetic field strength has been measured for the low-

PLATE 19

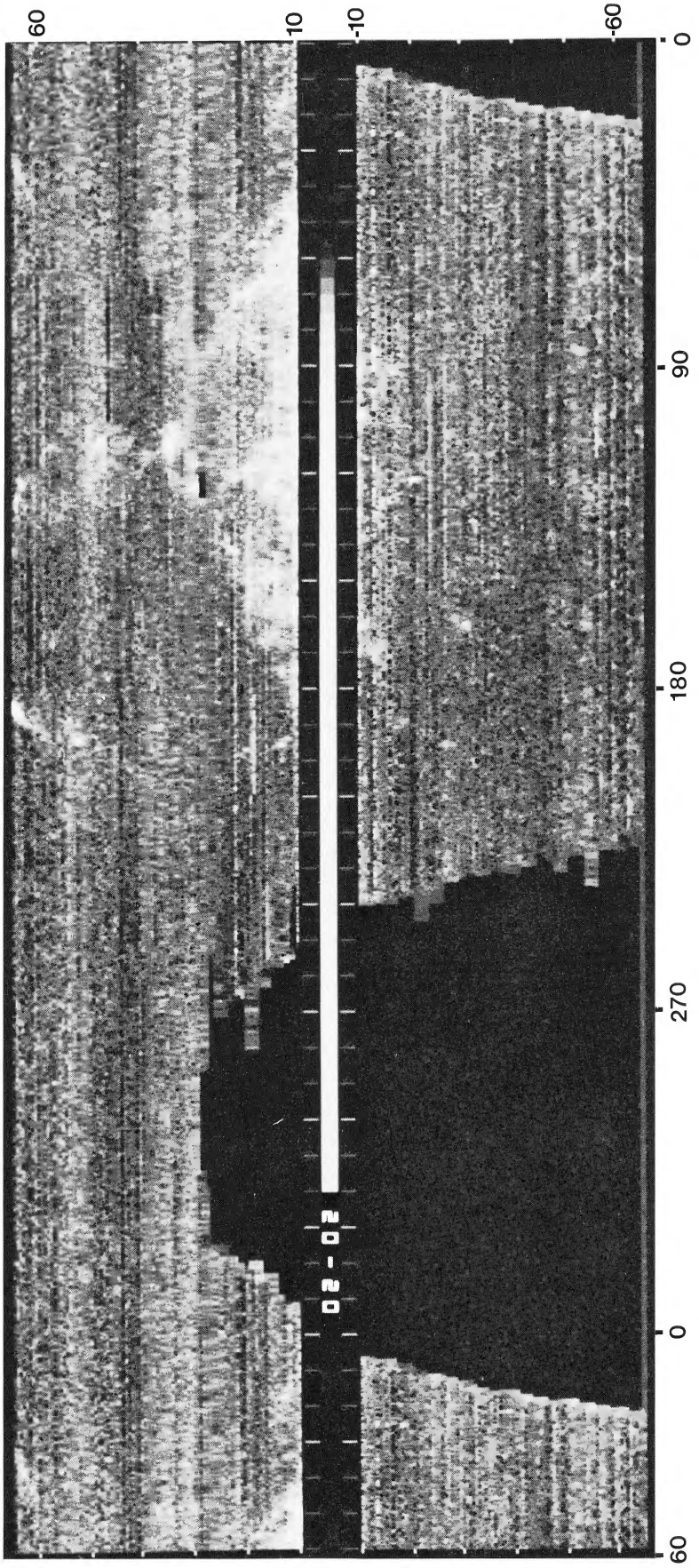

FIG. 2*a*.—Photographic representation of H I column density centered at LSR velocity -83.4 km s^{-1}; areas with larger column densities are whiter. Longitude increases from 0° at the right to 360° toward the left, then to 60° at the extreme left; there are tick marks every 10°, and heavy tick marks every 30°. Latitude increases from +10° in the middle to +65° at the top and decreases from −10° in the middle to −65° at the bottom; there are no data between latitude −10° and +10°. There are tick marks every 10° in latitude. There are no data below declination −30°.

HEILES (*see* page 587)

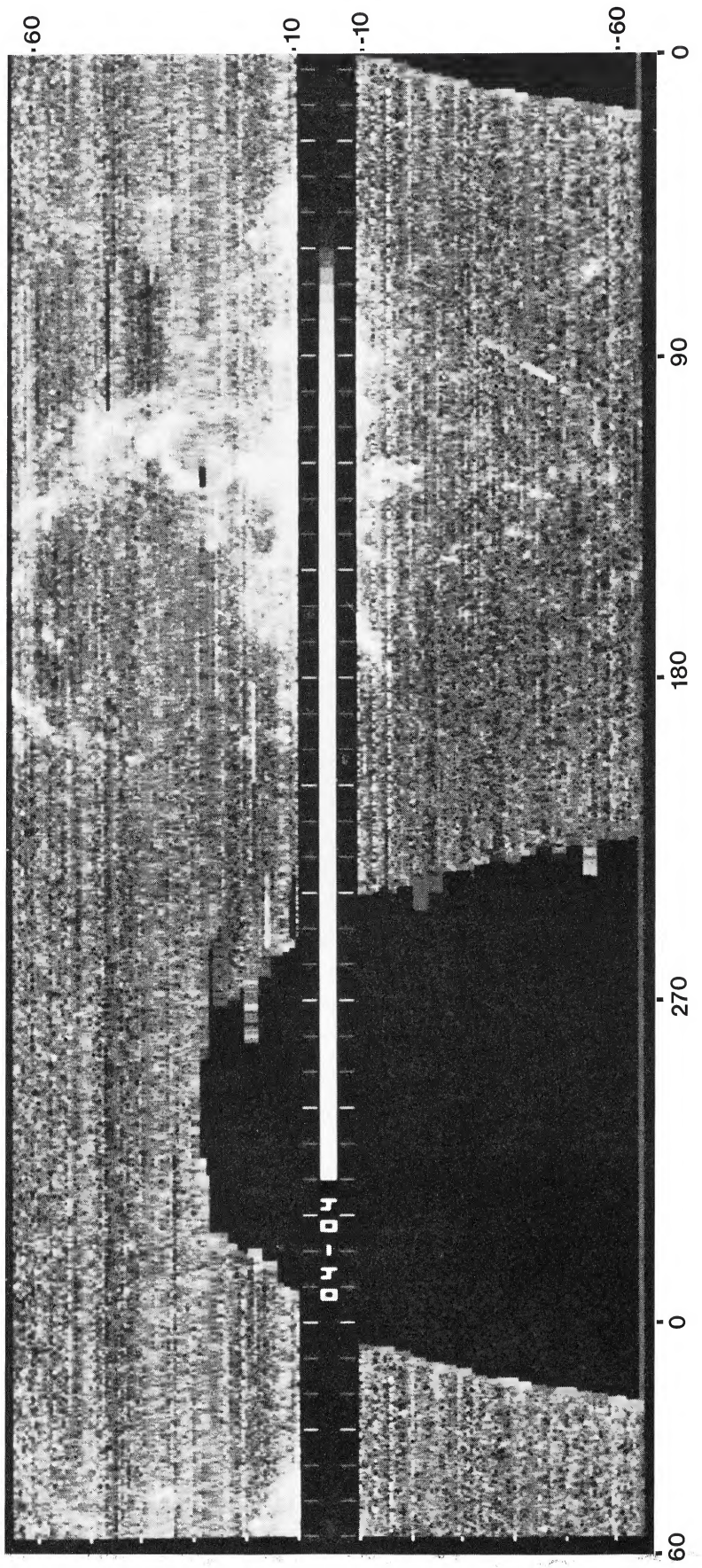

FIG. 2*b*.—Same as Fig. 2*a*, but centered at LSR velocity −70.7 km s^{-1}

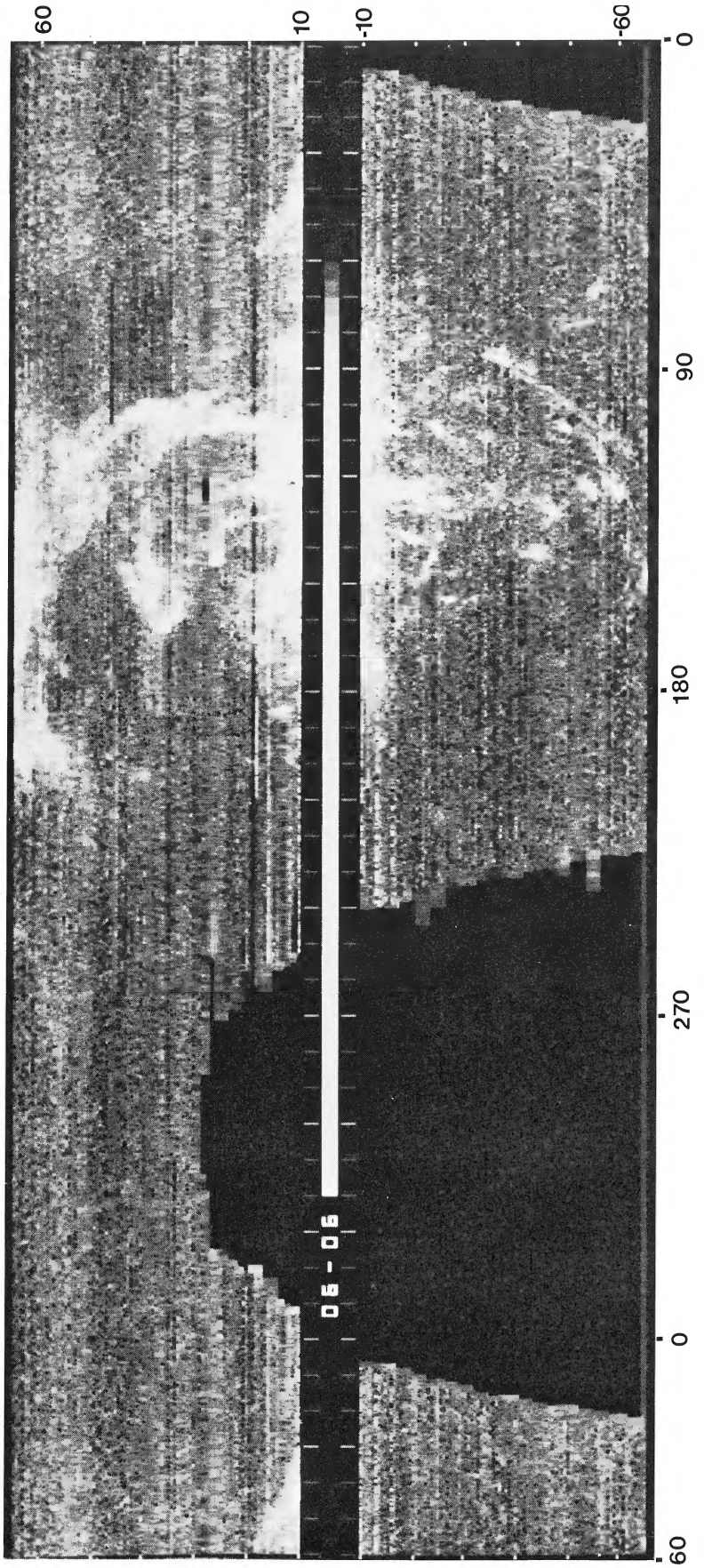

FIG. 2*c*.—Same as Fig. 2*a*, but centered at LSR velocity −58.1 km s^{-1}

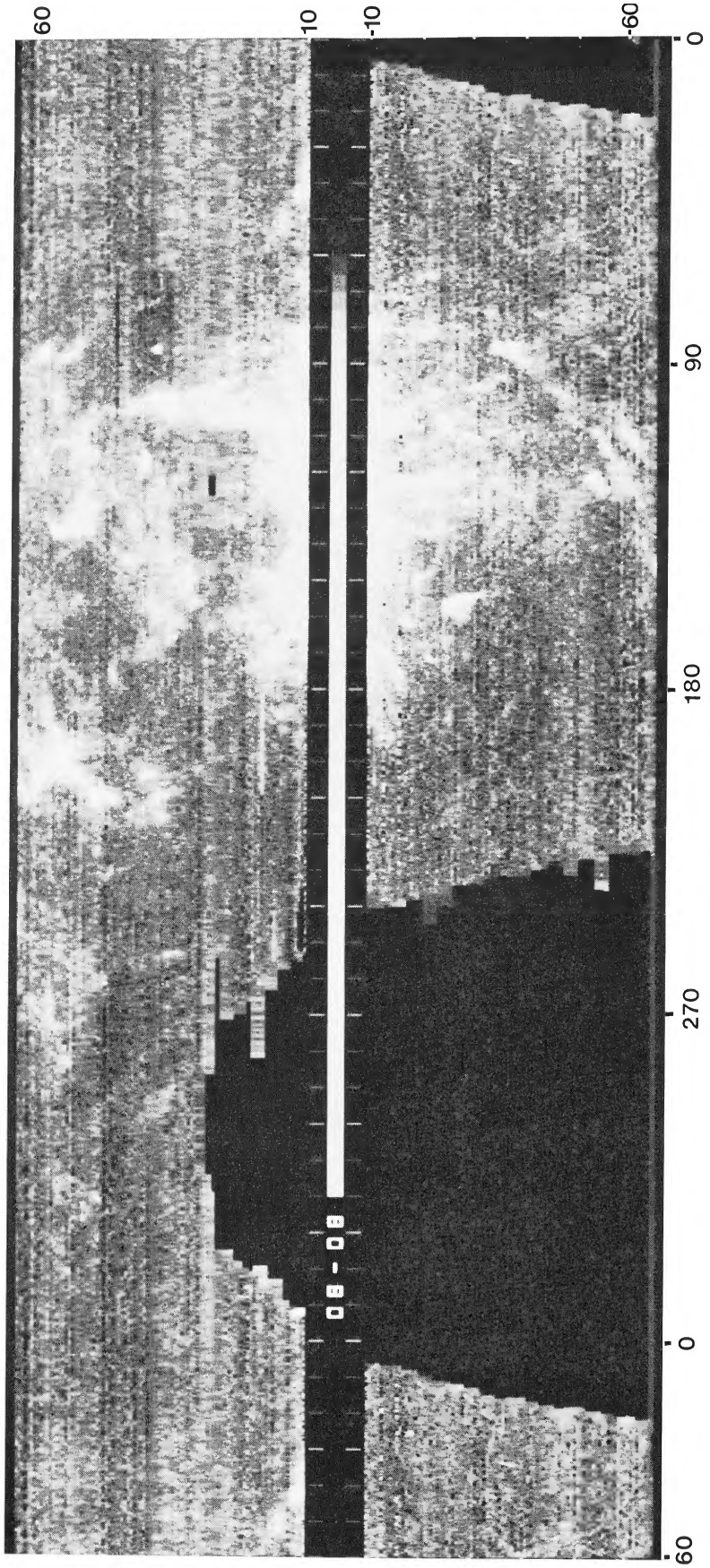

FIG. 2*d*.—Same as Fig. 2*a*, but centered at LSR velocity −45.4 km s^{-1}

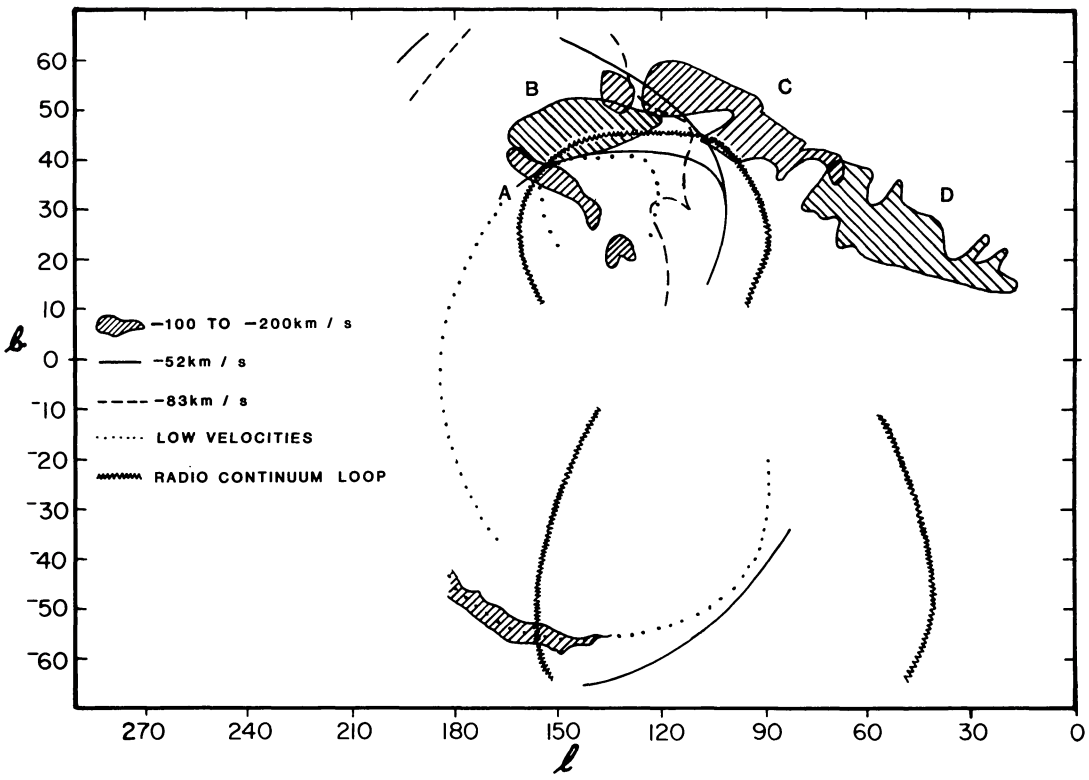

FIG. 3.—Sketch of the locations of selected H I ridge lines at high velocities, intermediate velocities, and low velocities, together with the radio continuum loops II (at negative latitudes) and III (at positive latitudes).

velocity gas at one position (Troland and Heiles 1982); its pressure dominates the gas pressure.

There might be high positive velocity gas associated with these structures. Bates *et al.* (1983) have detected gas at about $+70$ km s^{-1} in absorption against UV of stars, using *IUE* spectra. These stars are inside and, in one case, near the periphery of radio loop II; in this one case the line ratios imply a thin sheet of dense gas (thickness 0.1 pc, density 100 cm^{-3}) which suggests a fast shock. If this gas is really associated with the low-velocity and negative-velocity filaments, then a shell model is ruled out because gas near the periphery of a shell should have low velocities.

b) GS 155+38−58

This IV (~ -60 km s^{-1}) shell overlaps radio continuum loop III (Berkhuijsen, Haslam, and Salter 1971) and is somewhat larger in size, $\sim 105° \times 65°$ in l and b. It has a low column density, as does the IV gas near GS 120−30−8, and is only barely visible on Figures 1*c*–1*i*, which have fairly low contrast. It is more easily seen in Figures 2*a*–2*d*, which are at higher contrast and larger scale. These figures show that the gas is distributed in filaments that are roughly circular in appearance and have diameters of $\sim 80°$ for the higher negative velocities. There is velocity structure, with some tendency for the diameter to decrease as the velocity becomes more negative. The velocities of this gas, less negative than about -100 km s^{-1}, are those of the classical "intermediate-velocity" (IV) gas (see review by Verschuur 1975).

i) *Interpretation as an Expanding Shell*

Figure 2 suggests quite strongly to the eye that the IV gas resides in a spherical, expanding shell. An explosive origin for the IV gas has been postulated previously by Verschuur (1971) and by Wesselius and Fejes (1973), although the latter authors prefer a different model (see below). Both papers note that there is a deficiency of low-velocity gas whose column density is just about equal to that of the IV gas, and the latter authors used interstellar absorption lines to show that the IV gas is closer than 400 pc. Neither paper places the IV gas in such a large shell—70° in diameter—as is so strongly suggested by Figure 2.

The shell is still barely discernible at the velocity limit of the Heiles and Habing survey, -90 km s^{-1}. Fortunately, there exist other H I survey data that allow us to extend the velocity coverage; these are summarized in Figure 9 of Giovanelli (1980*a*). Figure 3 depicts some HV gas, denoted by Giovanelli as the "Northern HV Complex," with velocities between -200 and -100 km s^{-1}. In this figure, A, B, and C are traditional subdivisions, apparently based mainly on brightness, i.e., ease of detection; D was newly discovered by Giovanelli.

It is possible to interpret portion A of the HV gas, the IV filaments, and the low-velocity filaments as parts of the same expanding shell. This could happen if the physical shell has a very large expansion velocity, ~ 70 km s^{-1}. In this case, the systemic LSR velocity of the physical shell would be about -70 km s^{-1}. The low-velocity gas, having more positive

velocities ranging to the +12 km s^{-1} of GS 135+29+4, would be parts of the receding hemisphere, and portion A of the HV gas, with velocities of about −160 km s^{-1}, would be part of the approaching hemisphere. In this interpretation, we would be seeing both hemispheres of this very large, rapidly expanding shell. All of this gas, together with HV portions B and C, might be associated with radio loop III.

ii) *An Alternative Interpretation*

Alternatively, one can follow Wesselius and Fejes (1973) and forego the interpretation of a spherical shell for the IV gas, and any other gas, in this region. There are two justifications for this approach, despite the strongly suggestive curved appearances of the H I filaments at various velocities. The first comes from maps of the whole northern galactic hemisphere centered on the northern galactic pole, which do not exclude the region above latitude 65° as do our figures. These maps, especially one such as Figure 2*g* of Wesselius and Fejes (1973) which is centered at −28 km s^{-1}, show that H I occupies a large fraction of the upper half of the northern galactic hemisphere. In the "spherical shell" picture, one considers some of this gas to be separate and associated with the H I near radio loop I, while in this alternative view, one considers all of this gas to be physically related. The second justification for this alternative approach is the long tail, marked "D" in Figure 3, on the HV gas distribution. Giovanelli (1980) shows that this tail has a larger velocity scatter than the other portions of the HV gas, which may argue that it is physically distinct; on the other hand, it may be physically associated with the other HV gas because its velocity does fit smoothly onto that of component C. This changes the appearance of the HV gas filaments from a circle to a boomerang shape. The boomerang shape is not consistent with a spherical shell. This alternative view considers the whole IV/HV complex to be formed from an infalling cloud which accelerates the ambient, low-velocity gas to intermediate velocities, as may have also happened in the negative galactic hemisphere (see discussion of GS 120−30−8).

c) GS 174+02−64, the "Anticenter Shell"

This "anticenter shell" (Heiles 1983*a*, *c*) is ~30° in size and has a low column density; it is visible, but only with difficulty, over a large velocity range, from −89.7 to −21.6 km s^{-1} (Figs. 1*a*–1*k*). It exhibits some changes in size and appearance with velocity. Figure 4 shows high-contrast gray-scale representations of this shell at two velocities, −70.7 and −45.4 km s^{-1}; Figure 5 shows a single sketch that depicts the locations of the ridges at velocities between −90 and −45 km s^{-1}. On the photographs of Heiles (1979), which exhibit only $|b| < 10°$ but extend to much higher negative velocities, a portion of this shell—near $(l, b) = (162, 8)$—remains barely visible. On the diametrically opposite part of the shell near $(l, b) = (185, -11)$, Mirabel (1982) finds very high negative velocity (VHV) gas, between −200 and −100 km s^{-1}. Analysis of the Bell Laboratory's H I survey (Stark *et al.* 1983), currently underway, shows that velocities in this region reach at least −330 km s^{-1}!

This shell is located near the galactic anticenter. It is so large in angle, and has such a large negative velocity, that portions of it have been mistaken for a large-scale galactic feature at a "forbidden" velocity. Kepner (1970) described it as feature *Q*, and portions of O_i and possibly O_0. Dieter (1971) described it as part of an infalling shell of gas that supposedly defines the outer boundary of our Galaxy. Davies (1972) described it as high-velocity clouds trailing after spiral arms. Verschuur (1973) described it as spiral arms δ and Σ, which had to have noncircular motions. Weaver (1974) described it as a "jet"; in fact, it is often referred to as "Weaver's jet." Simonson (1975) described it as an external dwarf galaxy!

De Noyer *et al.* (1977) argued that some of this gas is relatively close and associated with the supernova remnants IC 443 and the Origem Loop. Burton and Moore (1979) and Moore and Burton (1979) also argued that some of the gas is local. However, the angular size of the sky mapped by all of these authors was insufficiently large to cover the full extent of GS 174+02−64. Watanabe (1984) examined a larger piece of sky and found structures which he interpreted as the collision of two shells. Watanabe's shells may be unrelated to GS 174+02−64, because they have an LSR velocity of +25 km s^{-1}; nevertheless, there might be physical association.

In our view, the circular structures strongly argue that the gas discussed by the authors referenced above, with the possible exception of Watanabe's shells at 25 km s^{-1} velocity, is part of the large shell-like object GS 174+02−64. There is no independent evidence for this object being a significant aspect of galactic structure, and we believe that its location near the galactic anticenter is simply a coincidence. However, we must note that even we may be underestimating the extent of this structure. Giovanelli (1980*b*) has found a 50° filament of H I at −115 km s^{-1} that runs from $(l, b) \approx (140, -8)$ to past the lower edge of GS 174+02−64. Further study is required to tell whether these objects are physically related.

The smaller scale studies of this object have revealed some apparent disturbances in the ambient galactic gas at the positions of small but prominent HV clouds. Moore and Burton (1979) and Burton and Moore (1979) show that an excess of HV gas at −140 to −30 km s^{-1} coincides with a deficiency of ambient gas in an area of several square degrees near $(l, b) = (197, 2)$. Mirabel (1982) finds a perturbation in the kinematics of the low-velocity gas in the vicinity of $(l, b) = (185, -11)$. These coincidences argue for a direct physical association of the high and low velocity gas. Mirabel discusses the physics of a possible collision of very high velocity gas with the ambient galactic gas and finds that a number of observational phenomena are reasonably accounted for. The probable source of very high velocity gas is fragmentation from the Magellanic Stream (see Mirabel's paper and the references quoted in the review of Heiles 1983*c*).

d) GS 193−32+4; GS 202−28+12

These shells are part of the Eridanus/Orion complex, which has been studied and discussed previously: in H I by Heiles (1976) and Hu (1981); in optical emission lines by Reynolds and Ogden (1979); and in soft X-ray emission by Naranan *et al.* (1976) and McCammon *et al.* (1983). The magnetic field strength in the Eridanus shell has been measured by Troland and Heiles (1982); magnetic pressure dominates gas pressure.

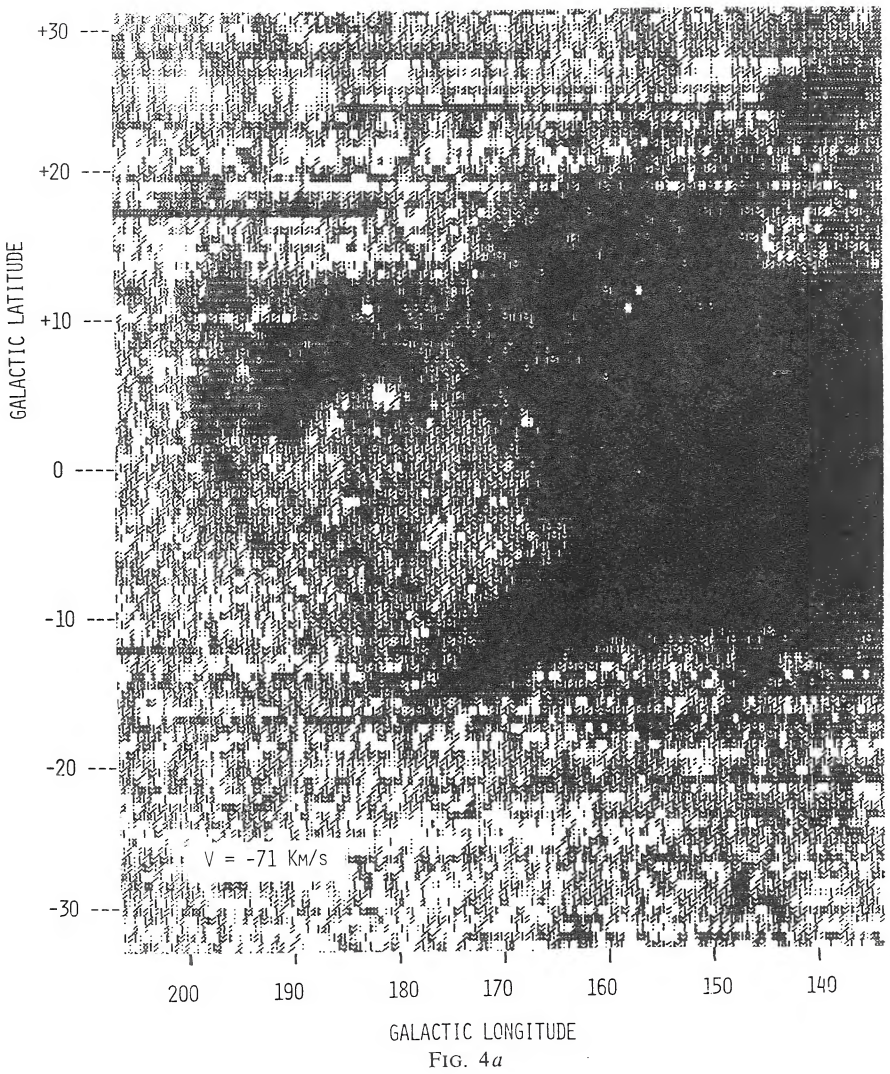

FIG. 4*a*

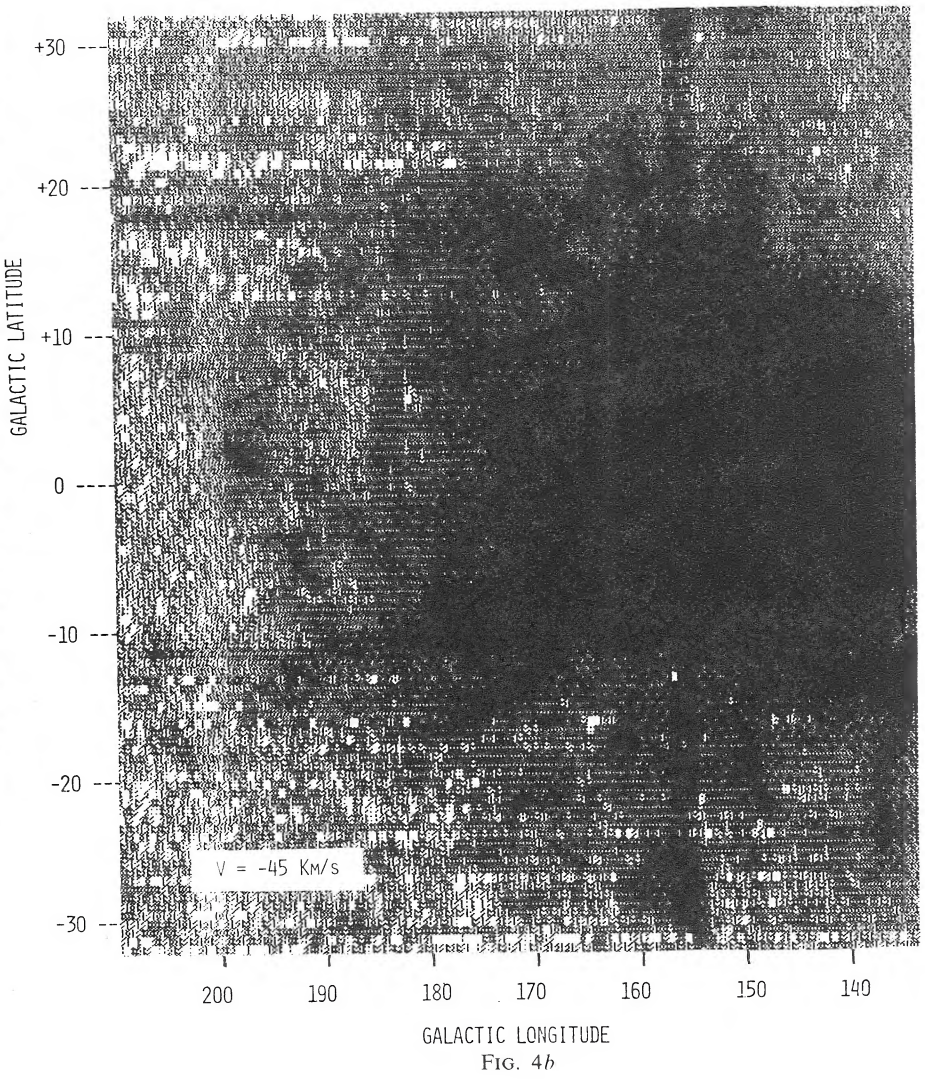

FIG. 4*b*

FIG. 4.—(*a*)–(*b*) Gray-scale representation of H I column density in the "anticenter shell" centered at velocities of −70.7 and −45.4 km s^{-1}; areas with larger column densities are blacker. The shell, denoted as GS 174+02−64 in Table 1, changes structure with velocity.

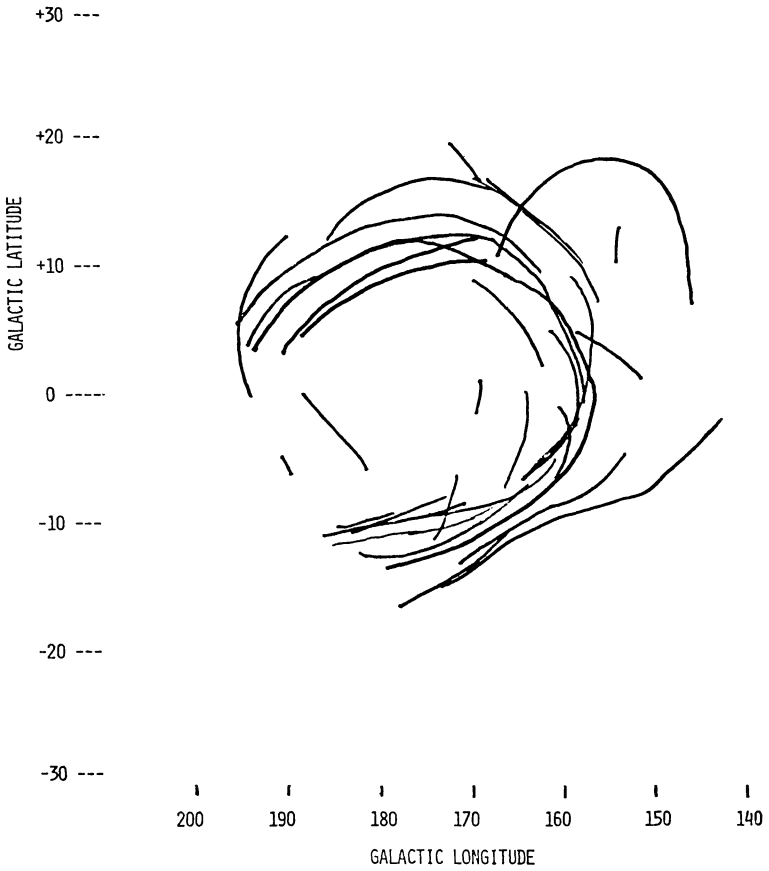

FIG. 5.—Sketch of the ridge lines of the H I filaments in GS 174+02−64 at velocities between −90 and −45 km s^{-1}

e) GS 331+14−15

This shell is not located in the area of sky covered by Figures 1 or 2. We list it here because it is the most prominent shell in the entire sky. It has a rather complicated H I structure which is best studied in the photographs of Colomb, Pöppel, and Heiles (1980). These photographs present H I data over the entire sky, derived from Hat Creek in the north and from the Argentine Institute for Radio Astronomy in the south.

The H I filaments in this vicinity increase monotonically in diameter from a velocity of about −30 km s^{-1} to about −4 km s^{-1}, where the angular diameter is ~120°. Within this velocity range there are occasional substructures, which also look like circular filaments. At positive velocities there are other filaments, which are either smaller in diameter or are centered at different positions. The filaments are weaker at the positive velocities, and some are only barely discernible on the pictures of Colomb *et al.* because of the poor quality and small scale of reproduction. Therefore, in Figure 6 (Plates 23–26) we reproduce four of these photographs, centered at −6, +8, +17, and +25 km s^{-1}. Portions of the shells in this region can be traced all the way to +34 km s^{-1}, the upper velocity limit of the Colomb *et al.* photographs.

The sizes of the H I filaments at negative velocities change in just the way expected for an expanding shell. This, together with the existence of circular filaments over such a wide velocity range, implies that the shell is expanding at ~25 km s^{-1}. This is in contrast to Weaver's (1979) statement that the shell is expanding at only 2 km s^{-1}, which was based on examination of the northern hemisphere data alone.

This shell lies just outside of radio loop I (the North Polar Spur); this region was recently reviewed by Heiles *et al.* (1980). The near edge is very close to the Sun (Crutcher 1982), even closer than the 120° diameter would imply. The simultaneous presence of a cold H I shell and hot, X-ray emitting gas in the interior implies the occurrence of more than one injection of energy from stellar explosions or stellar winds (Iwan 1980; Cox and Anderson 1982; Davelaar, Bleeker, and Derenberg 1980). The H II region of the many hot stars in the Sco/Oph associations may have produced the H I shell, in the manner envisaged by Beltrametti, Tenorio-Tagle, and Yorke (1982) and Tenorio-Tagle *et al.* (1982). Weaver (1979) believes that there is a significant difference between the center positions of the radio loop and the H I shell; however, the difference is much smaller than the angular diameters and may well not be meaningful.

f) Are Radio Loops II and III and the Low, Intermediate, and High Velocity Gas Filaments in Their Vicinities Part of a Single Huge, Coherent Structure?

Weaver (1979) has suggested that radio loops II and III, together with the associated intermediate and high velocity

PLATE 23

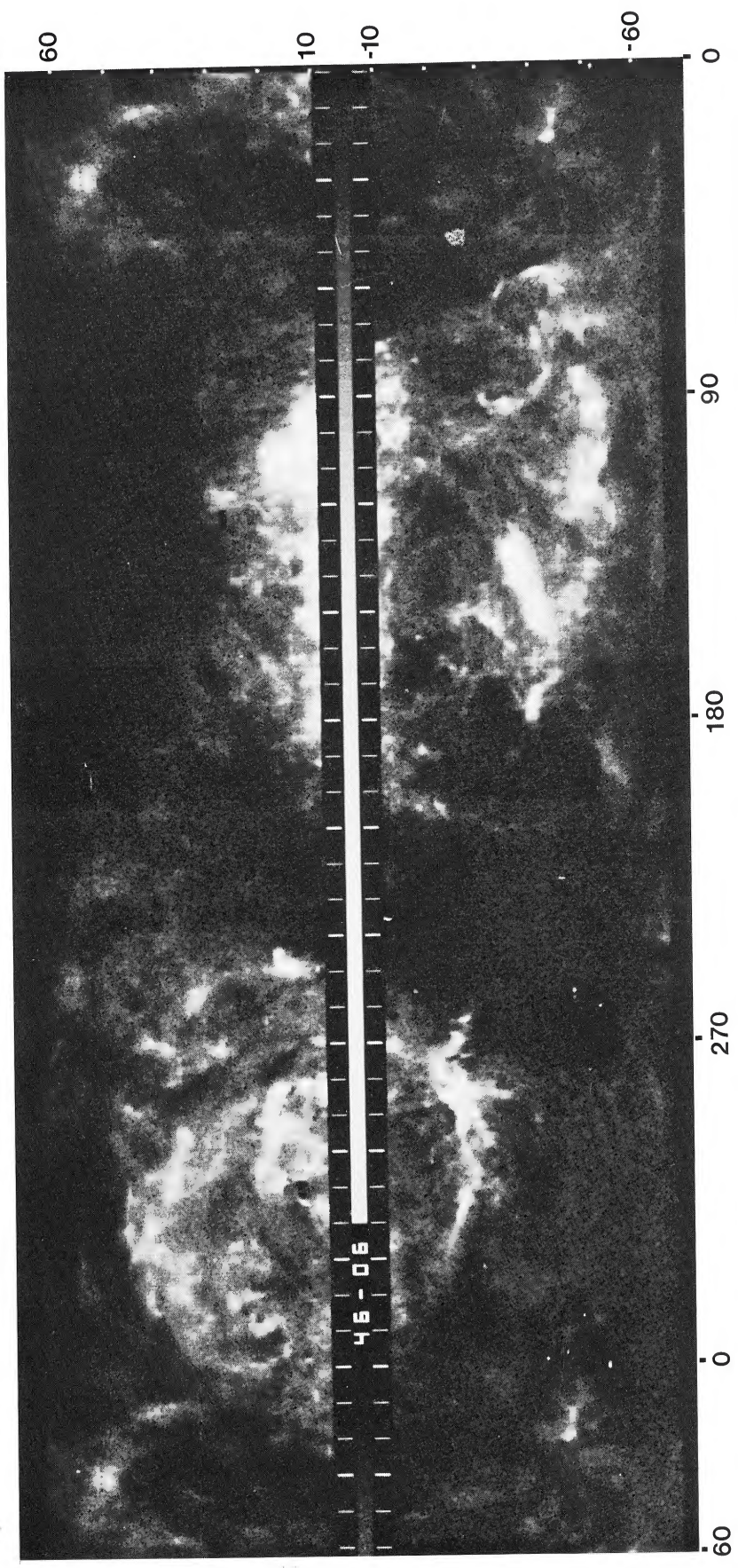

FIG. 6*a*.—Photographic representation of H I column density centered at LSR velocity -6.3 km s^{-1}; areas with larger column densities are whiter. As in Fig. 2, longitude increases from 0° at the right to 360° toward the left, then to 60° at the extreme left; there are tick marks every 10°, and heavy tick marks every 30°. Latitude increases from +10° in the middle to +65° at the top and decreases from −10° at the middle to −65° at the bottom; there are no data between latitude −10° and +10°. There are tick marks every 10° in latitude.

HEILES (*see* page 591)

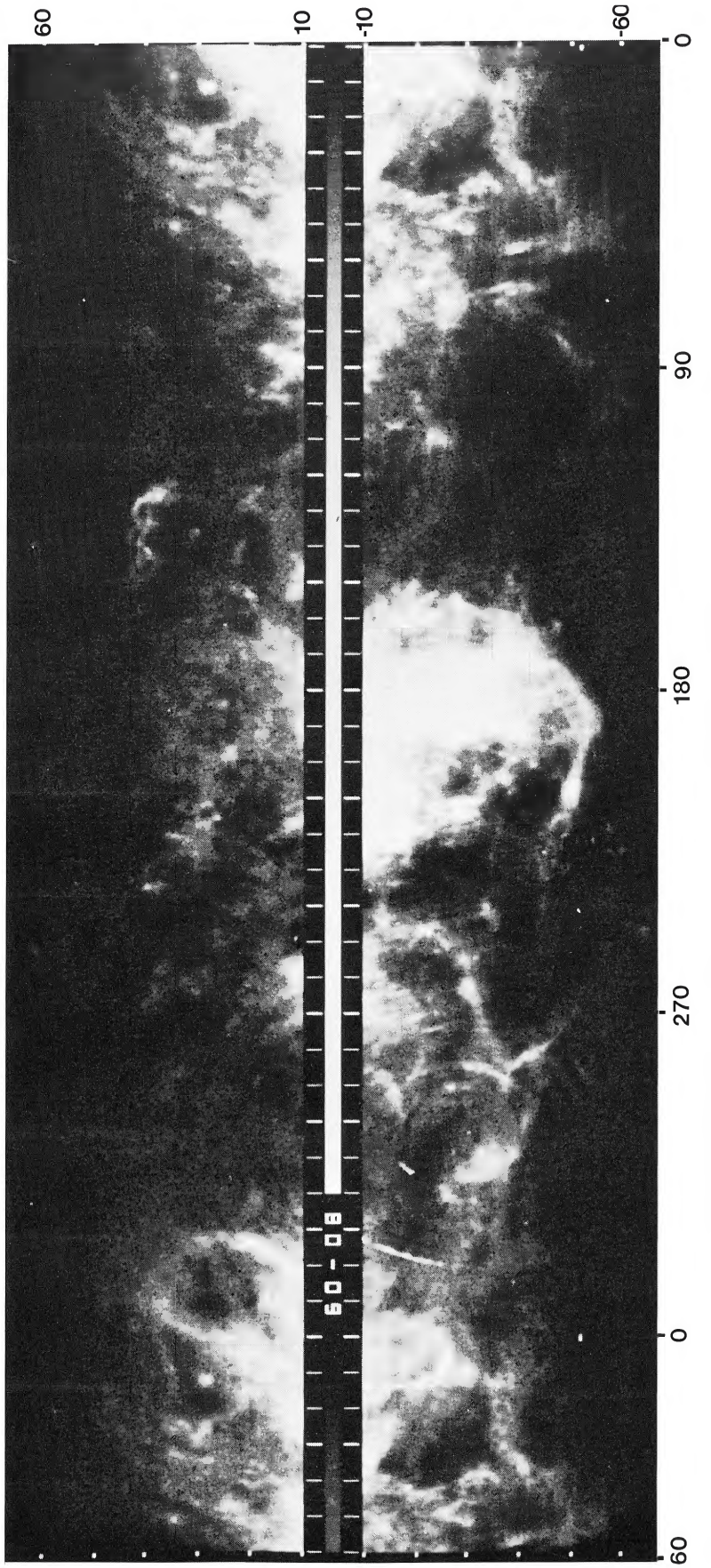

FIG. 6*b*.—Same as Fig. 6*a*, but centered at LSR velocity +8.4 km s^{-1}

PLATE 25

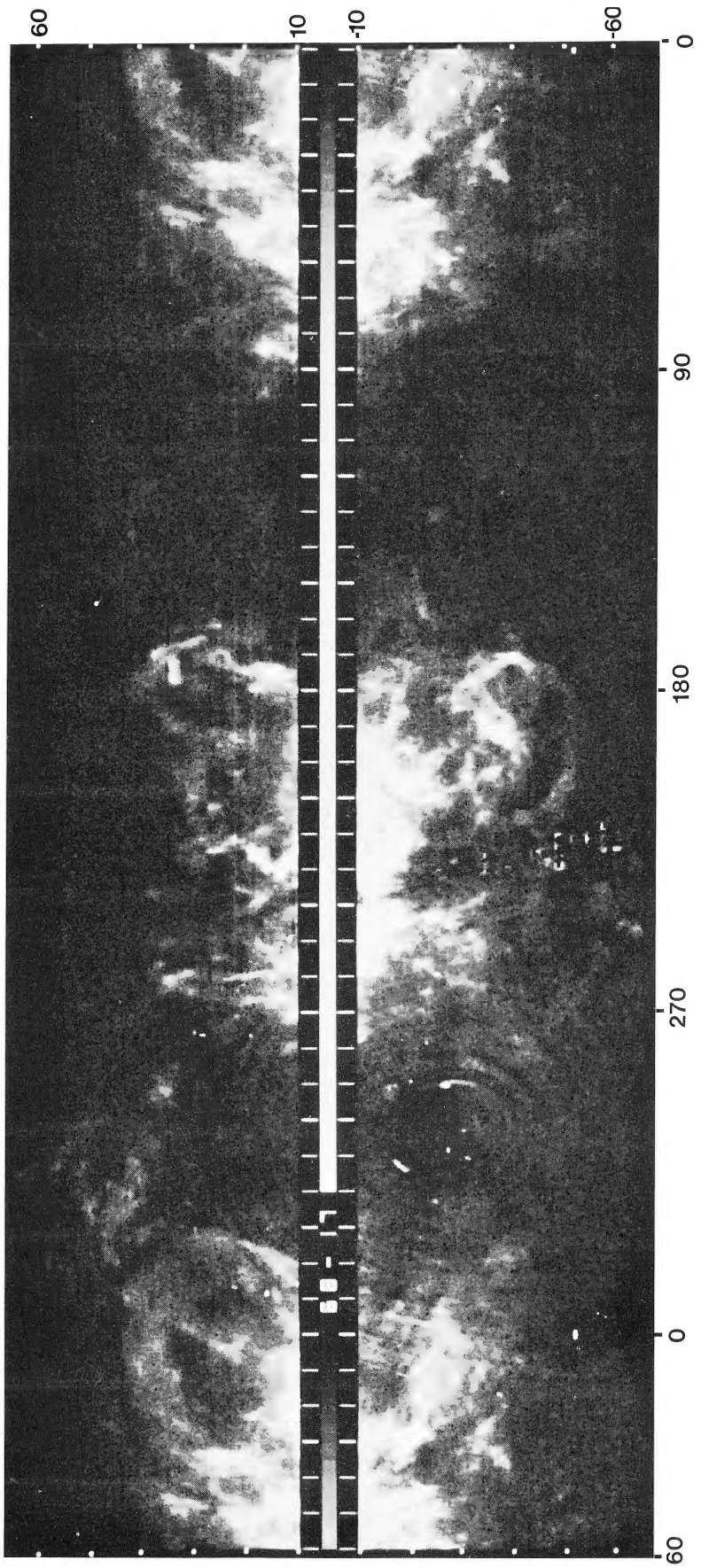

FIG. 6c.—Same as Fig. 6a, but centered at LSR velocity +16.9 km s^{-1}

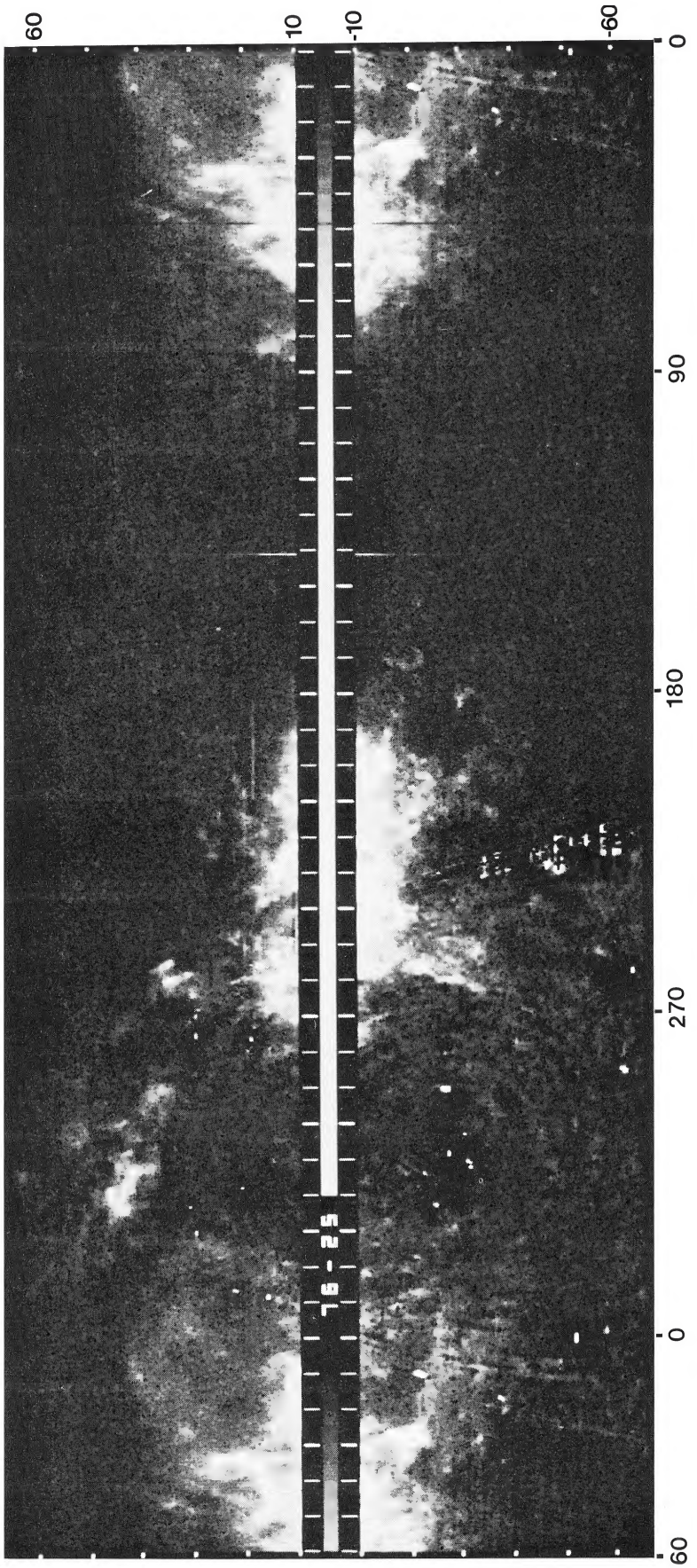

FIG. 6*d*.—Same as Fig. 6*a*, but centered at LSR velocity +25.3 km s^{-1}

HEILES (*see* page 591)

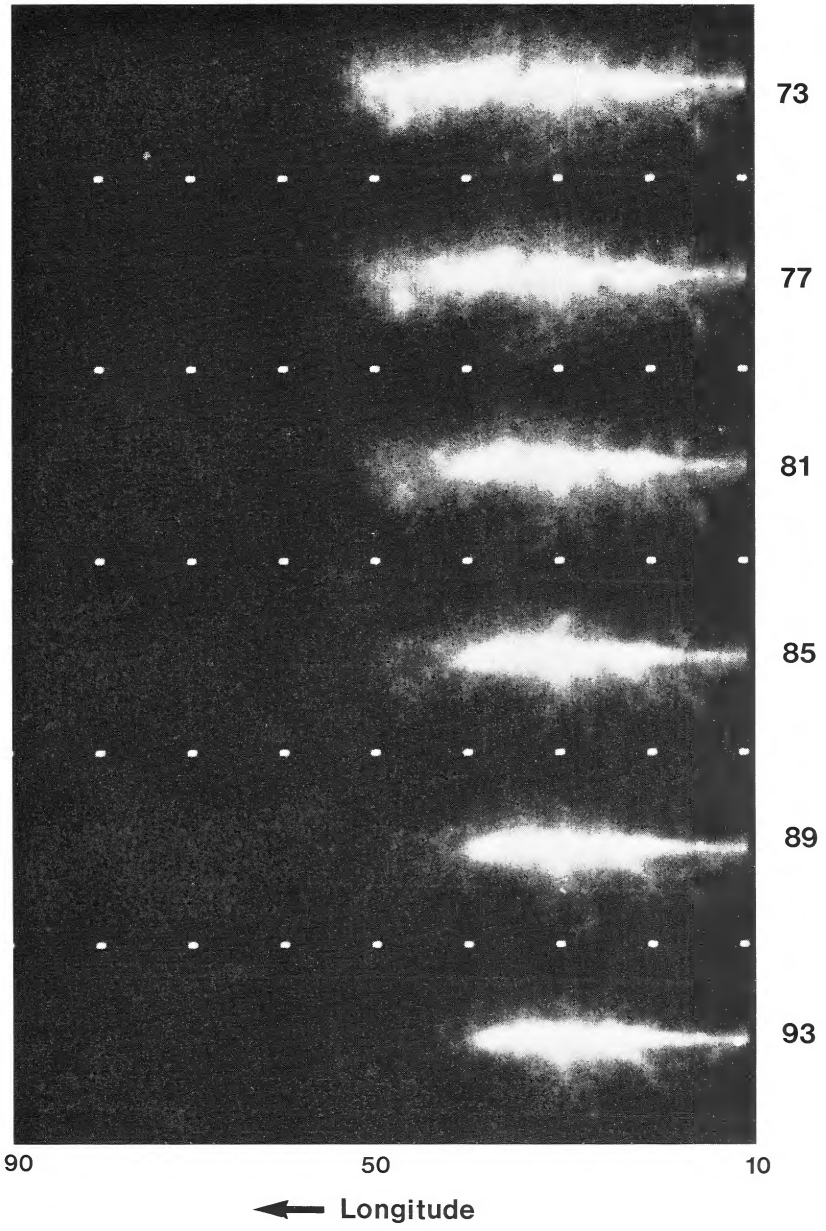

FIG. 7*a*

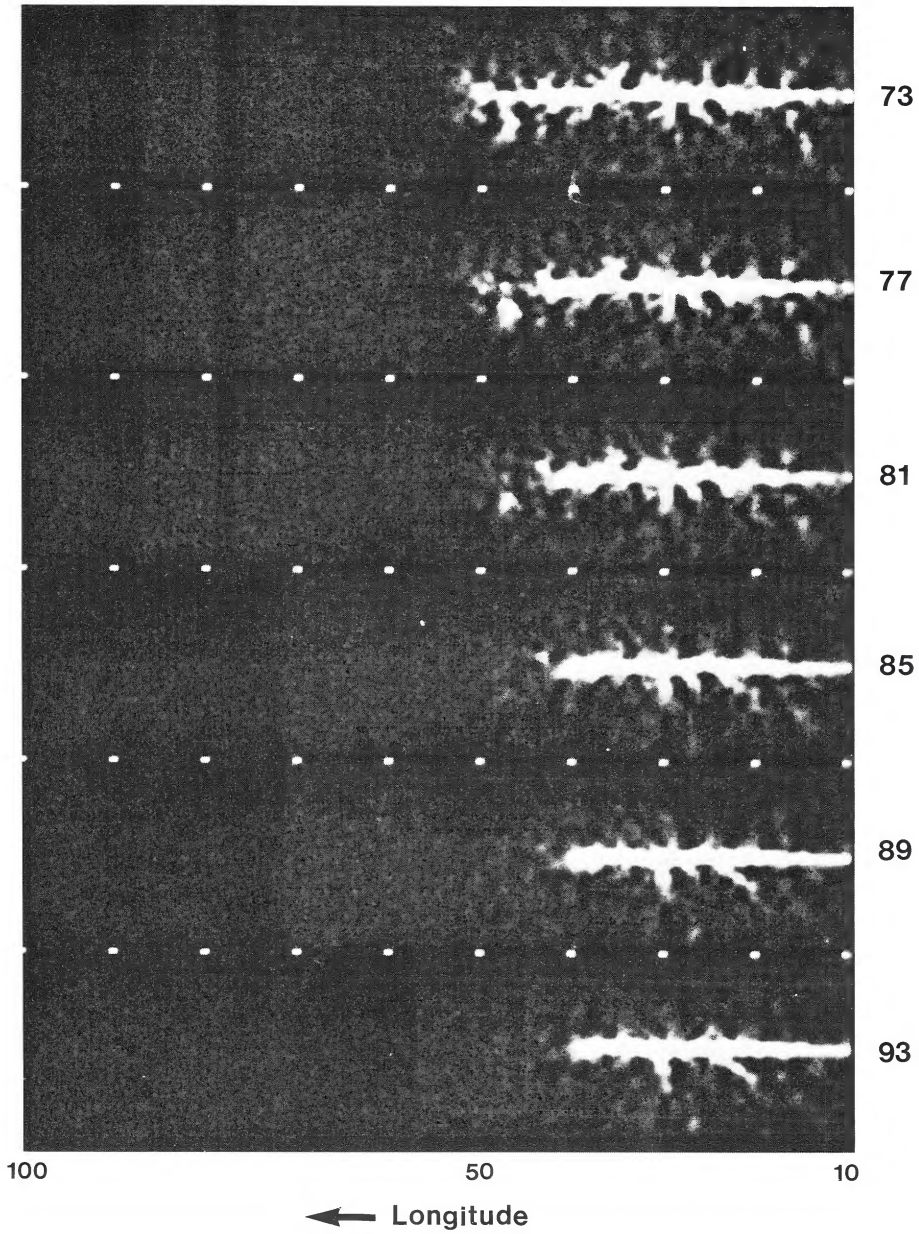

FIG. 7*b*

FIG. 7.—(*a*) Six pictures of the H I line intensity toward the inner galaxy in 2 km s^{-1} wide velocity intervals, spaced 4 km s^{-1}, for the interval 93 to 73 km s^{-1}. In each picture, longitude increases from right to left as indicated, and latitude increases from $-10°$ at the bottom to $+10°$ at the top. The central velocity appears at the right-hand side edge of each picture. The white tick marks appear every 10° in longitude. (*b*) Same data as shown in Fig. 7*a*, but after filtering to enhance small-scale structure as described in the text.

HEILES (*see* page 591)

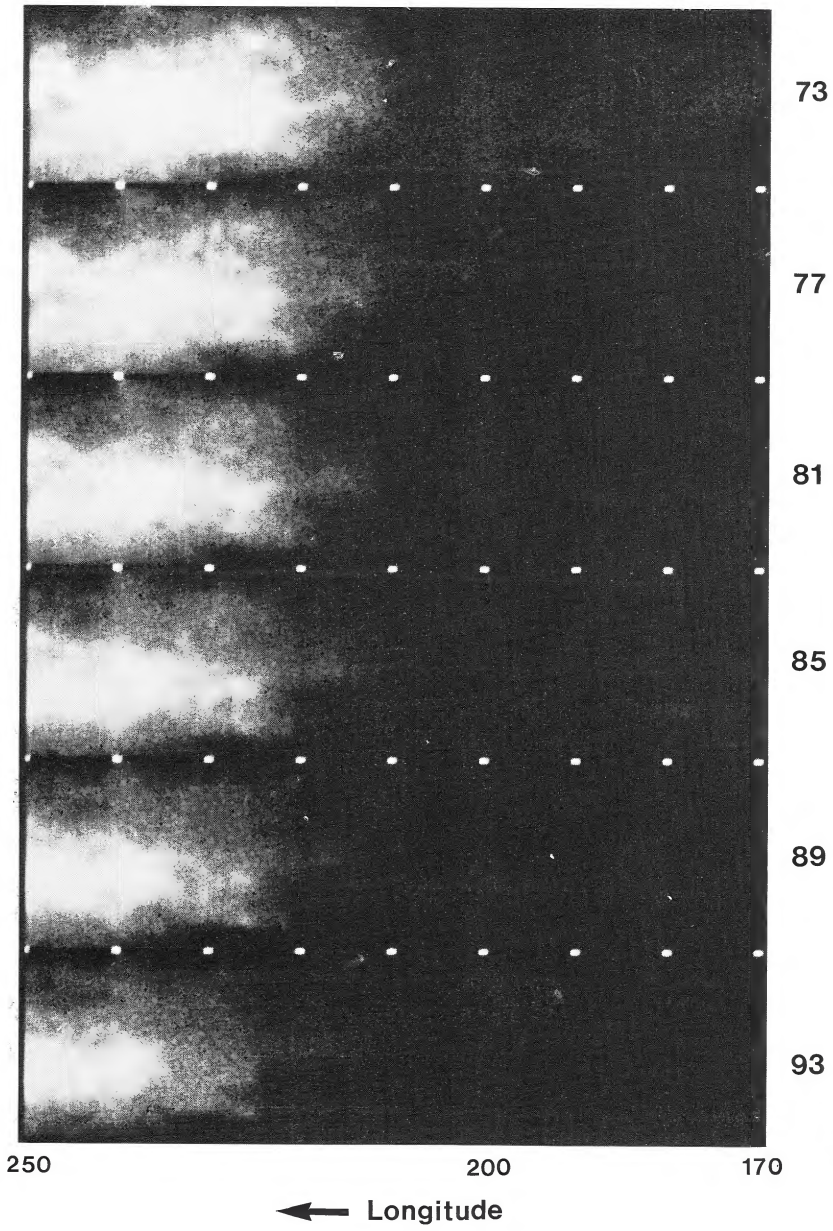

FIG. 7c

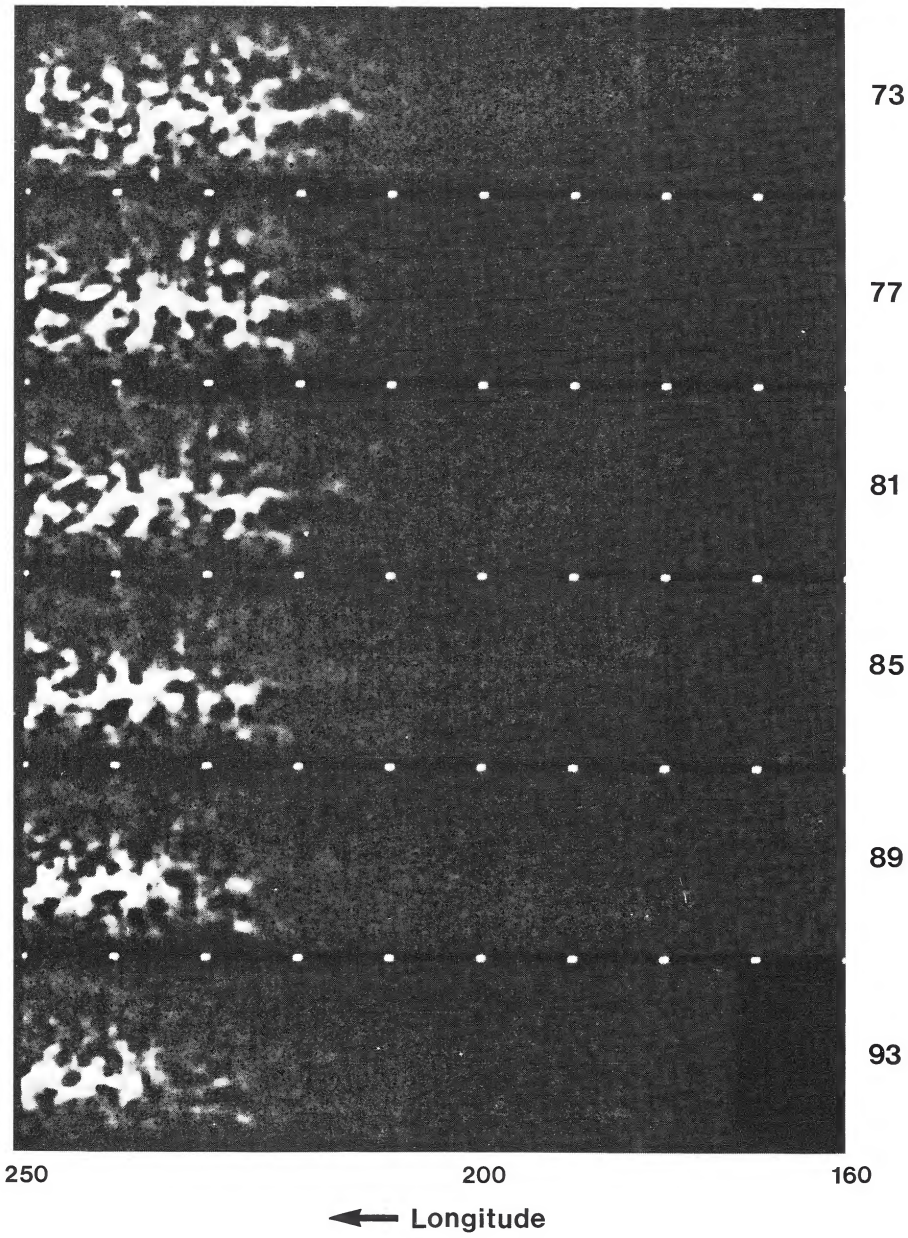

FIG. 7d

FIG. 7.—(*c*) Same as Fig. 7*a*, but toward the outer galaxy. (*d*) Same data as Fig. 7*c*, but after filtering to enhance small-scale structure.

HEILES (*see* page 591)

PLATE 28

PLATE 29

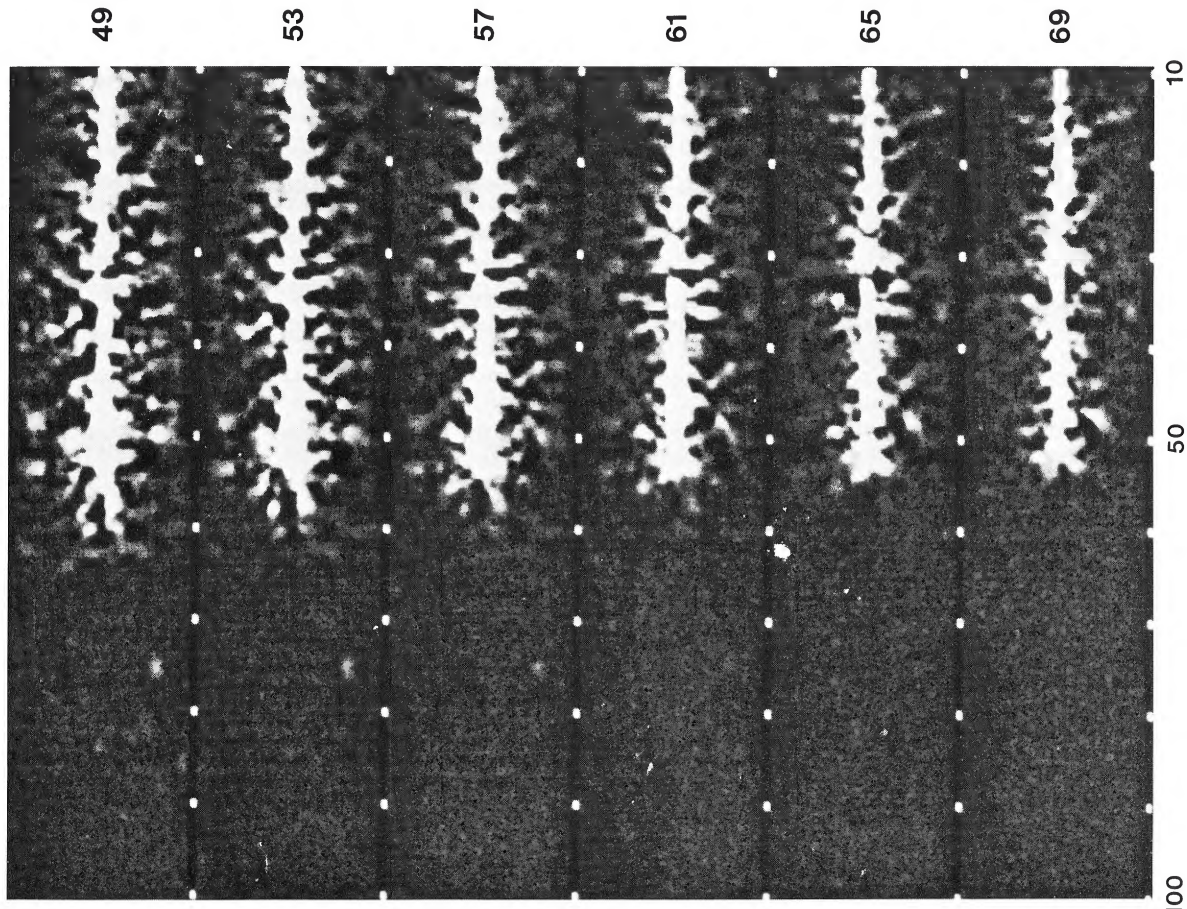

FIG. 8b

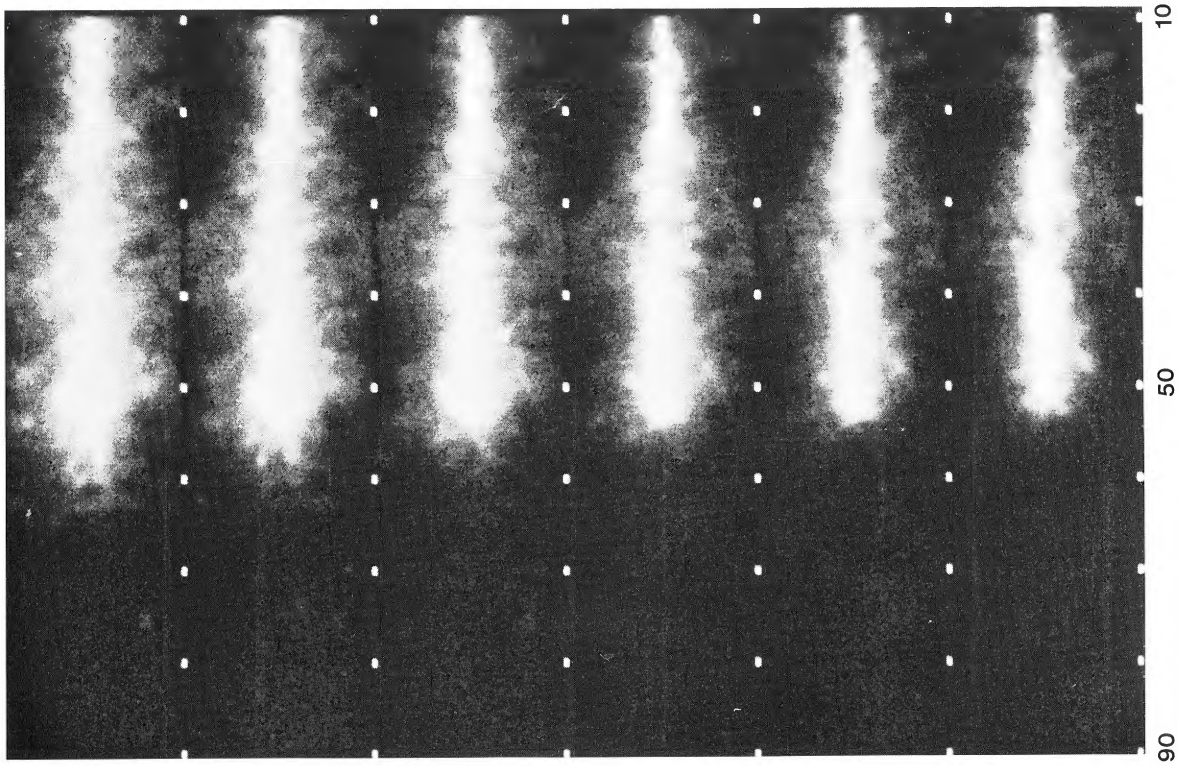

FIG. 8a

FIG. 8.—(*a*) Same as Fig. 7*a*, but for the velocity interval 69 to 49 km s^{-1}. (*b*) Same data as shown in Fig. 8*a*, but after filtering to enhance small-scale structure.

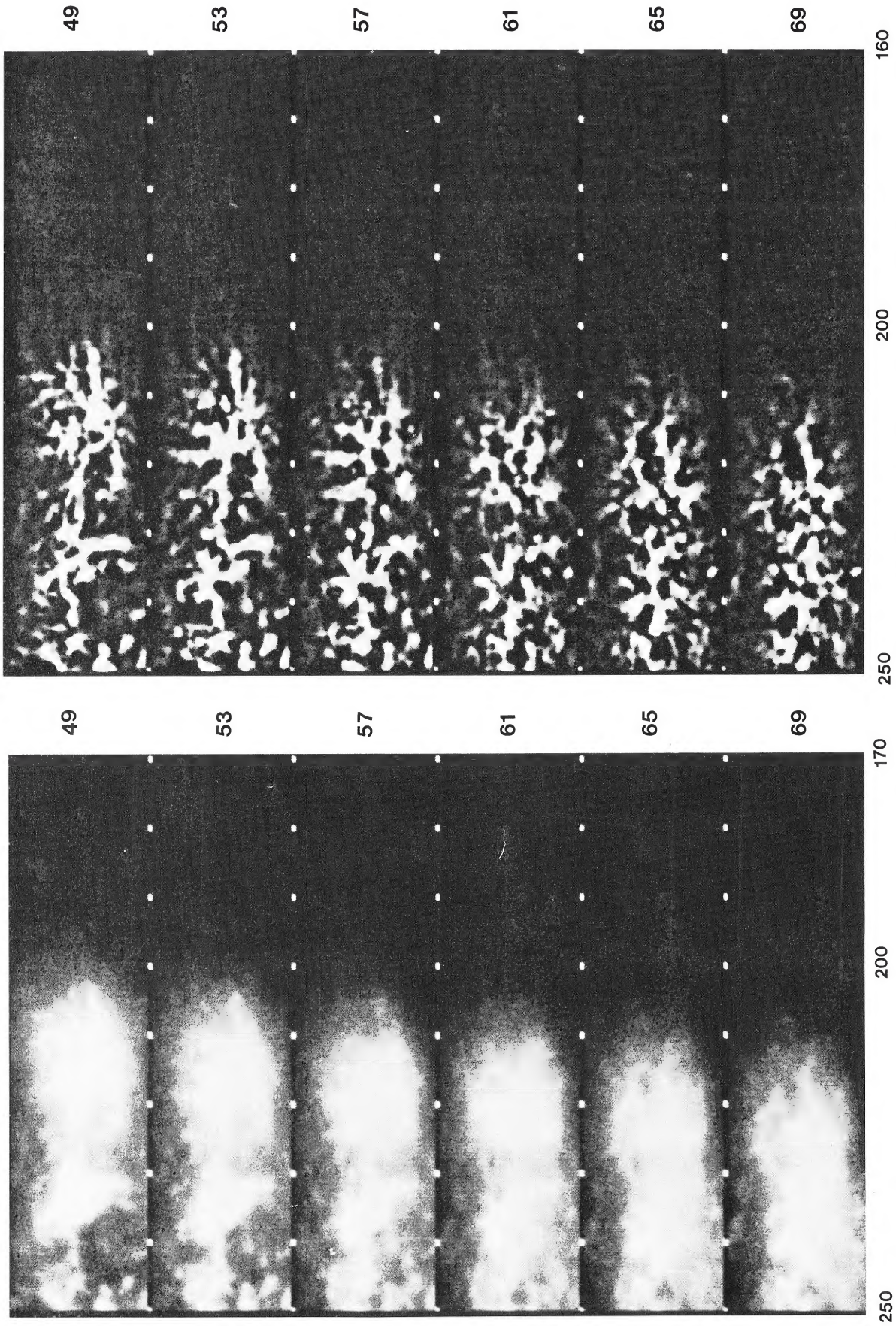

FIG. 8.—(*c*) Same as Fig. 8*a*, but toward the outer galaxy. (*d*) Same data as Fig. 8*c*, but after filtering to enhance small-scale structure.

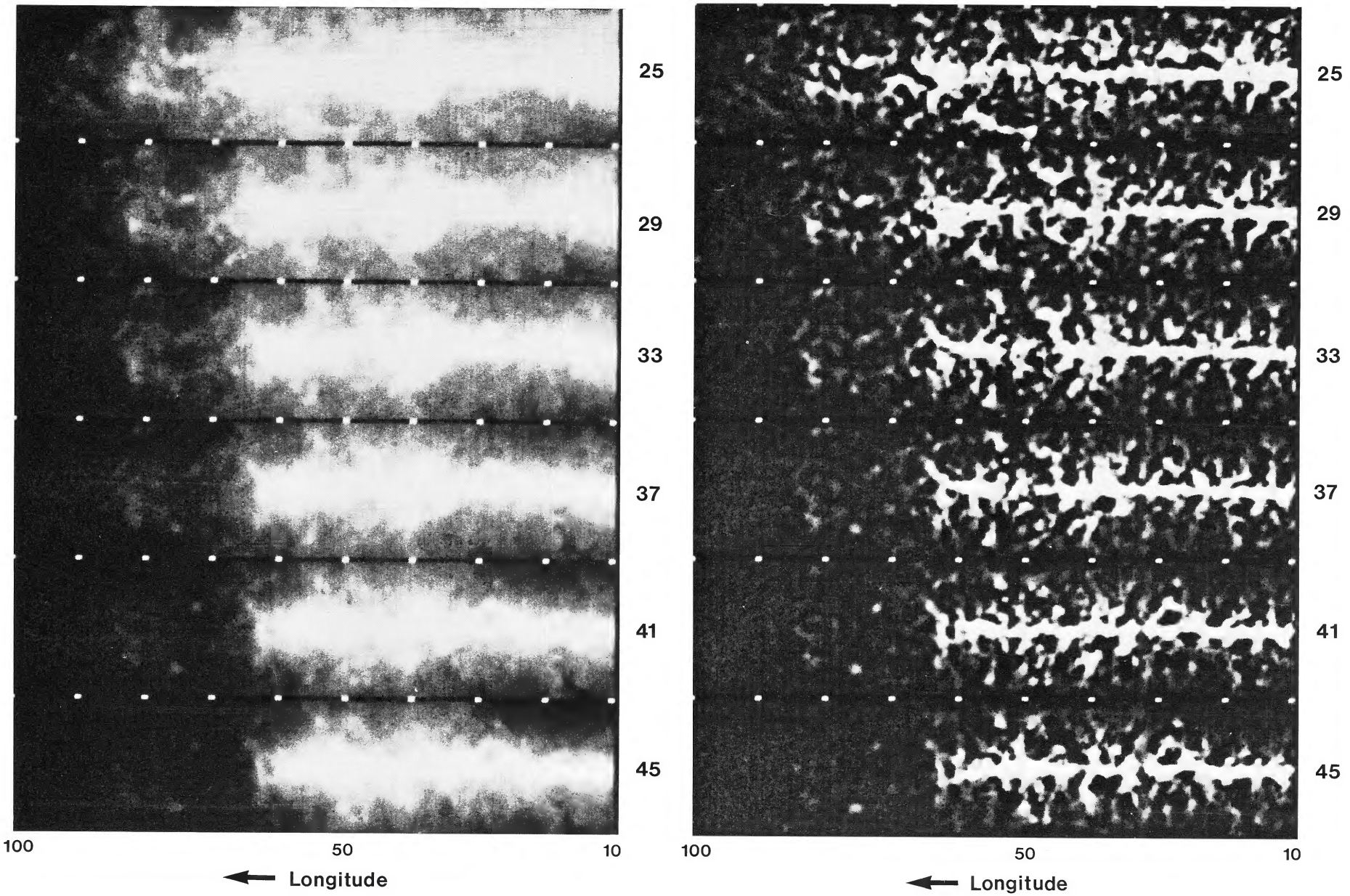

FIG. 9*a*

FIG. 9*b*

FIG. 9.—(*a*) Same as Fig. 7*a*, but for the velocity interval 45 to 25 km s^{-1}. (*b*) Same data as shown in Fig. 9*a*, but after filtering to enhance small-scale structure.

HEILES (*see* page 591)

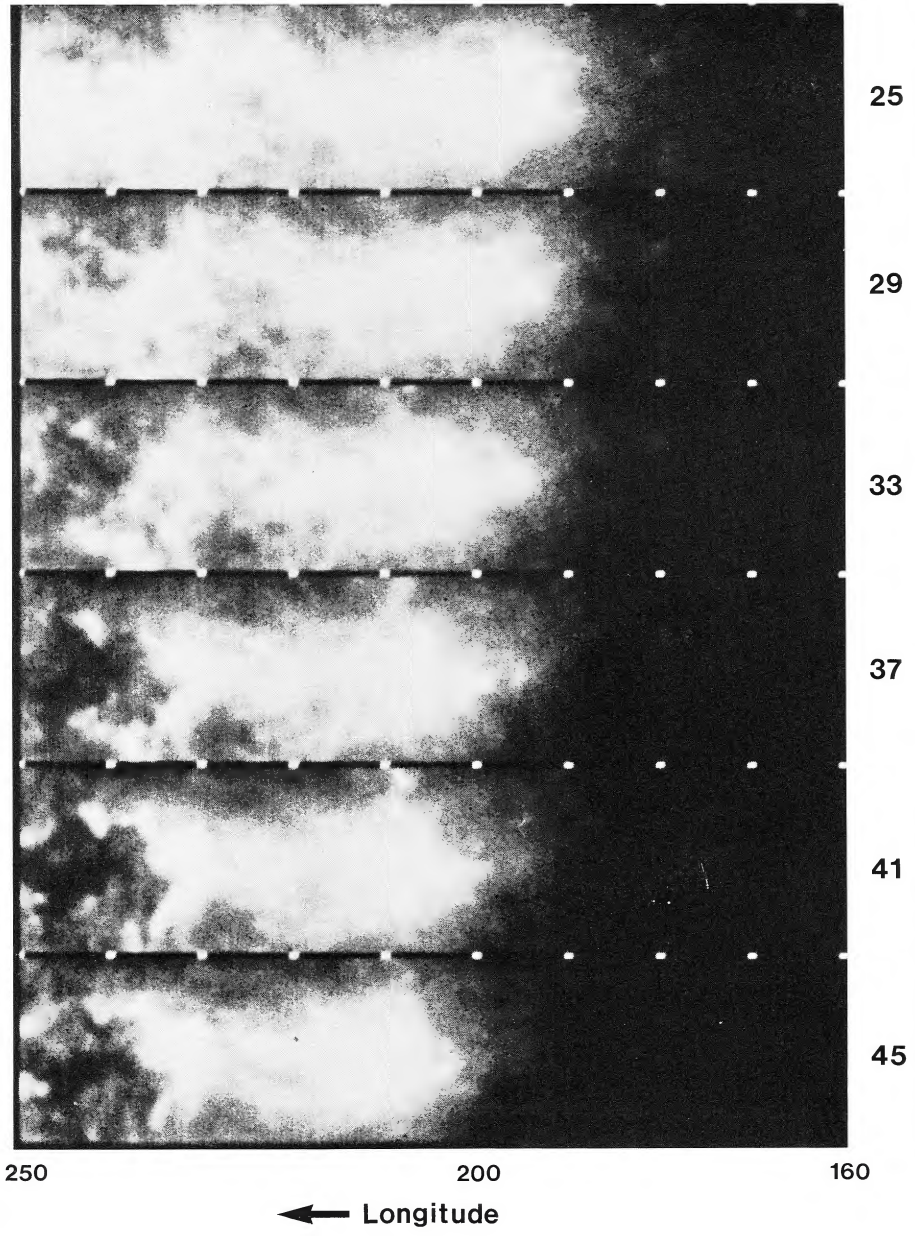

FIG. 9c

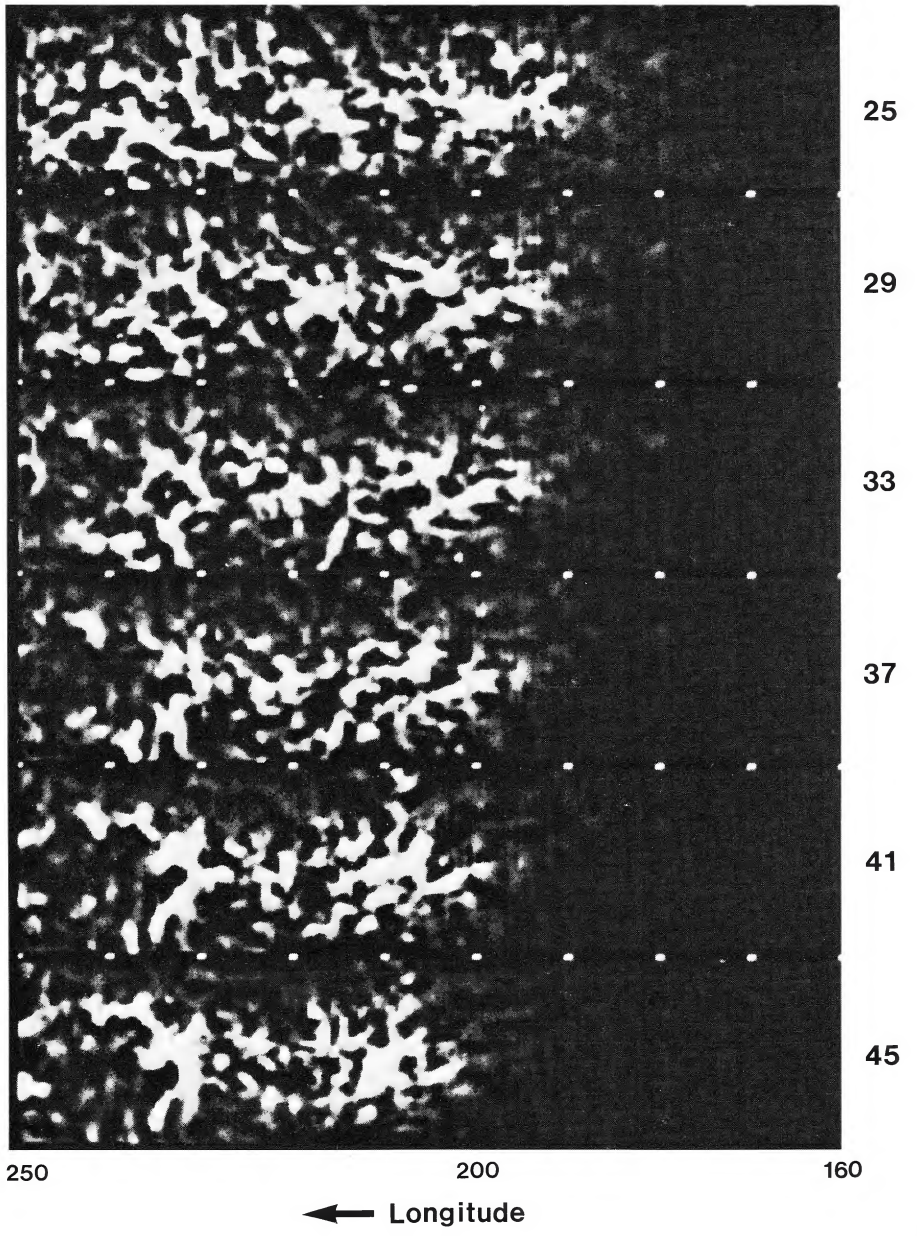

FIG. 9d

FIG. 9.—(*c*) Same as Fig. 9*a*, but toward the outer galaxy. (*d*) Same as Fig. 9*c*, but after filtering to enhance small-scale structure.

HEILES (*see* page 591)

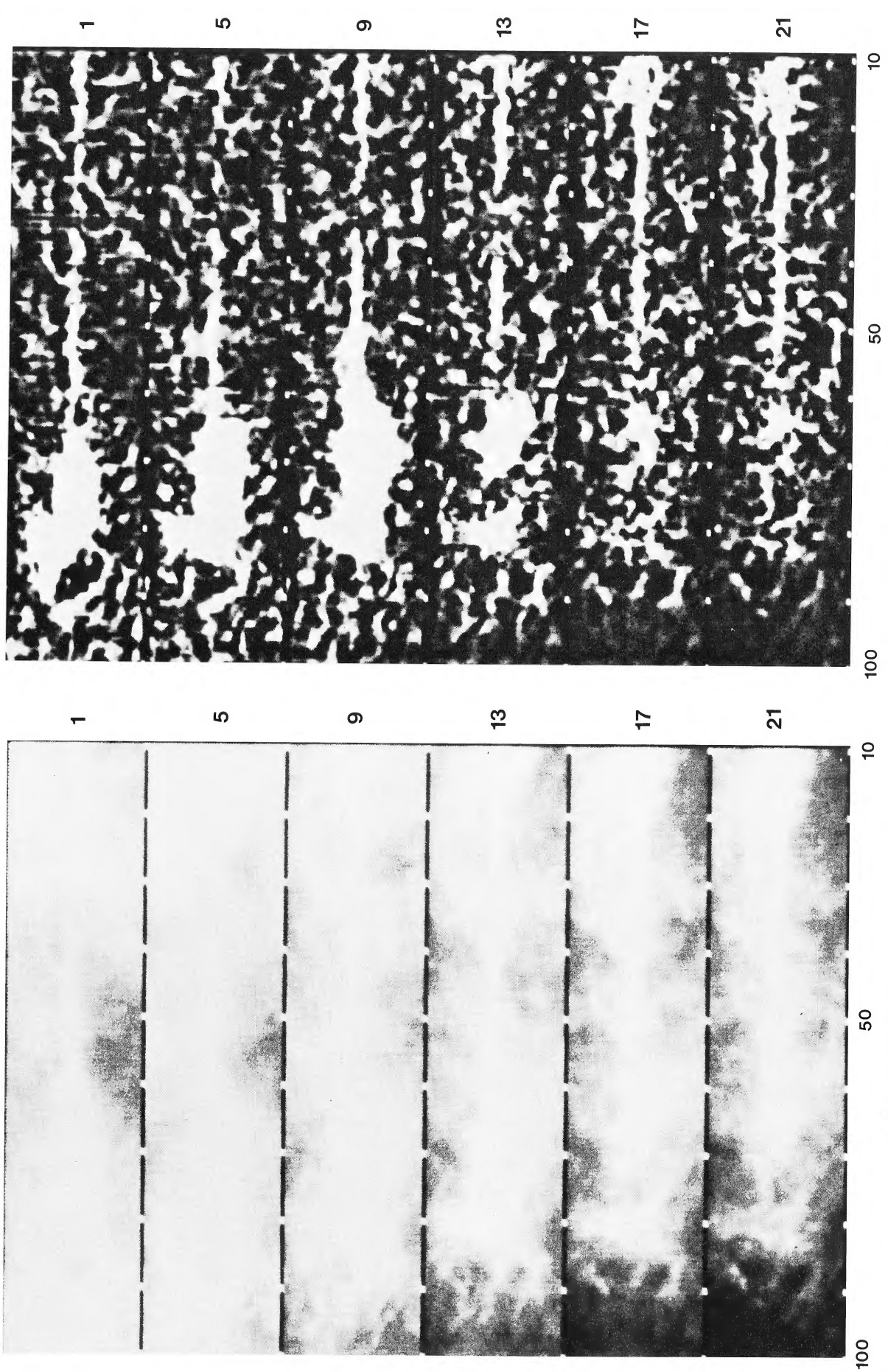

FIG. 10*b*

FIG. 10*a*

FIG. 10.—(*a*) Same as Fig. 7*a*, but for the velocity interval 21–1 km s^{-1}. (*b*) Same data as shown in Fig. 10*a*, but after filtering to enhance small-scale structure.

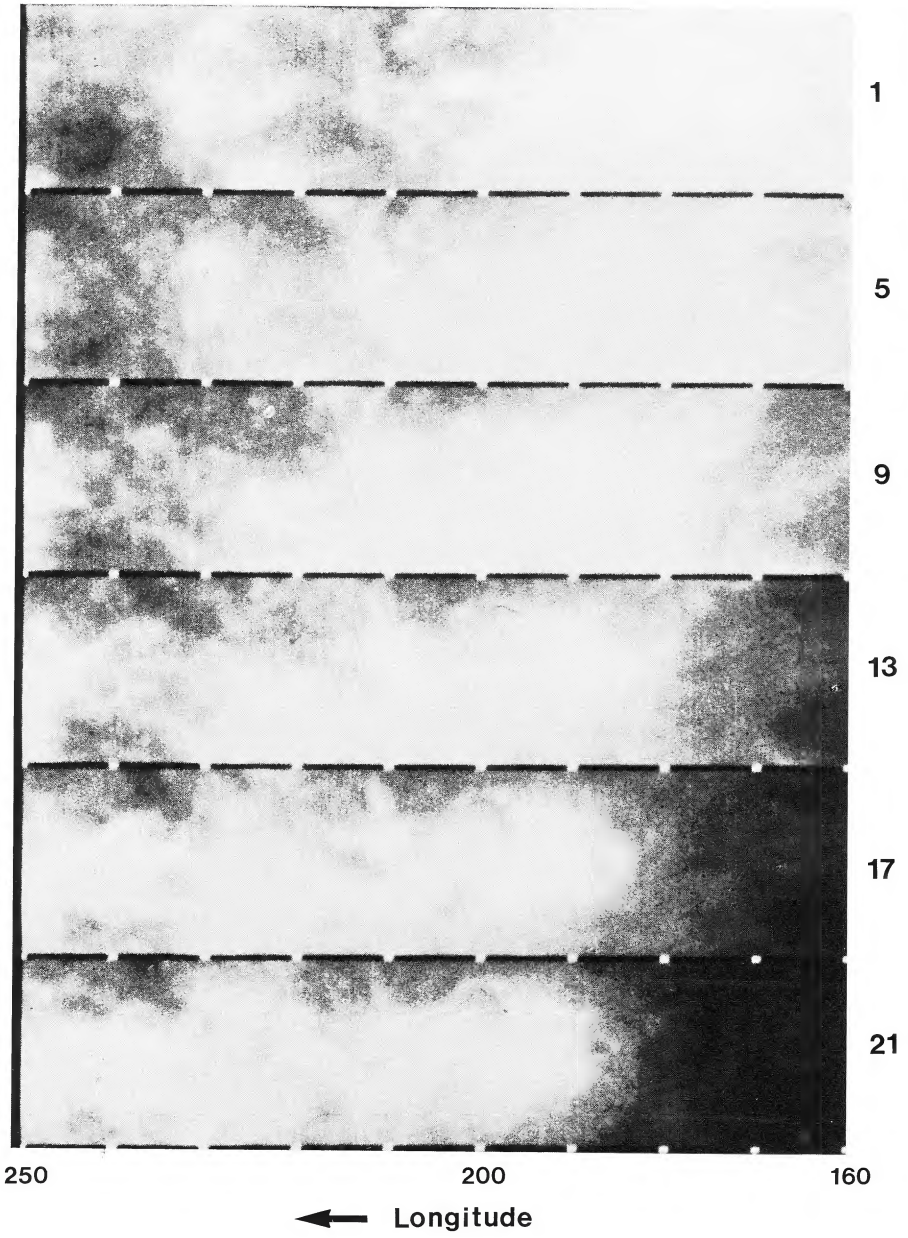

FIG. 10*c*

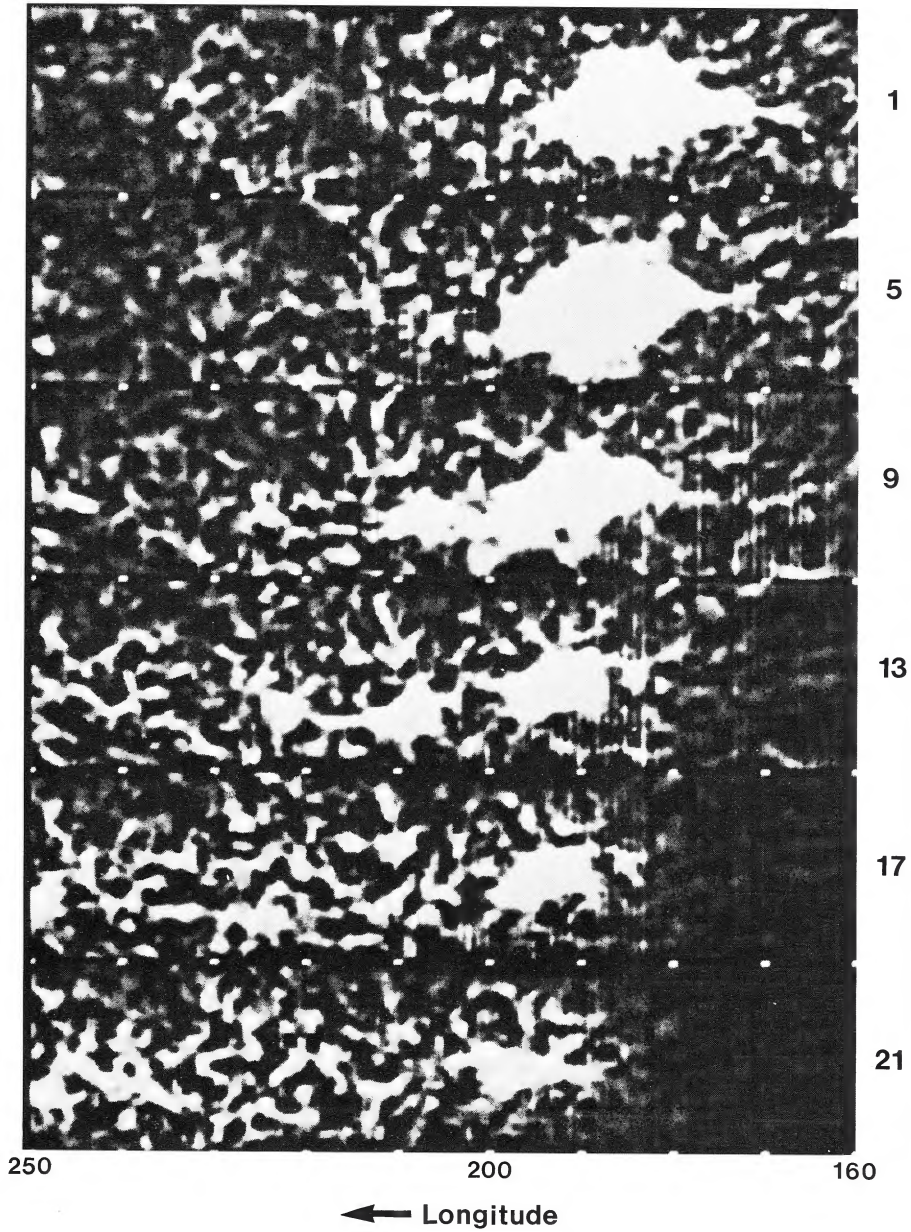

FIG. 10*d*

FIG. 10.—(*c*) Same as Fig. 10*a*, but toward the outer galaxy. (*d*) Same as Fig. 10*c*, but after filtering to enhance small-scale structure.

HEILES (*see* page 591)

H I ridges at both negative and positive latitudes, are part of one and the same physical object. This object would have been produced by stellar winds, supernovae, or both, in the Per OB3 association, located 150 pc distant at $(l, b) = (147, -5)$. Figure 3 shows the relative locations of all of these features, together with some low-velocity gas ridge lines in addition. This figure shows that the structures at positive latitudes are centered at higher longitudes than those at negative latitudes, typically by $\sim 30°$; however, since the angular diameters of the objects are so large, this displacement may not be significant and may only indicate that the expansion of material was asymmetric, presumably because the ambient material was not originally homogeneously distributed in space. These features may also be related to the expanding ring of gas in the solar neighborhood (see Olano 1982, and references quoted therein).

If one is willing to go so far as to accept Weaver's (1979) suggestion, then one might go somewhat further (Heiles 1983*b*) and include some of the low-velocity gas filaments as well, namely, those sketched on Figure 3. At negative latitudes, a low-velocity gas filament is coincident with a HV gas filament along part of its length, as discussed above in § III*a*. And at positive latitudes, a low-velocity H I ridge (best seen on Fig. 1*o* at $+12.7$ km s^{-1}) butts up against an IV ridge line (-52 km s^{-1}; see Fig. 2*c*) at the letter "A" in Figure 3. All of these structures are circular and centered, within an accuracy of 20°, at the same point.

If all of these structures are part of a single, coherent shell, then it is a most impressive shell indeed. The angular diameter would be $\sim 120°$, and its expansion velocity ~ 80 km s^{-1}. Its overall systemic velocity would be about -70 km s^{-1}. With such a large systemic velocity it is difficult to envision how it could have been produced by release of energy from an object imbedded within the ambient medium. Rather, the collision of infalling gas with ambient gas or perhaps some other mechanism that can transfer significant momentum to the ambient gas is needed.

IV. "WORMS"

We have used spatial filtering (Heiles 1983*c*) to enhance small-scale structure to facilitate the study of distant H I structures. Our first efforts have been restricted to the galactic plane H I survey of Weaver and Williams (1973) and the inner galaxy where the problems are most severe. This survey has an angular resolution of 0°.5. At each velocity, the survey data were smoothed by computing the median in a square box 3° on each side. The smoothed data were subtracted from the original data. This has the effect of emphasizing features having angular structure smaller than 3° in one direction.

The results are shown in Figures 7–10 (Plates 27–34), which are photographic presentations of both spatially filtered and unfiltered H I in l, b space at different positive LSR velocities. At positive velocities, there is no H I for longitudes between 90° and 180°, where galactic rotation produces "forbidden" positive velocities. Below $l = 90°$, positive velocities show gas in the inner galaxy; above $l = 180°$, they show gas in the outer galaxy.

Casual inspection of these figures shows that there is a qualitative change in structure toward the inner galaxy. In Figures 7*d*, 8*d*, 9*d*, 10*b*, and 10*d*—i.e., outside galactocentric radius 8.6 pc—the outer galaxy appears to be random, showing no preferred direction and showing rapid changes with velocity. In contrast, the structure in Figures 7*b* and 8*d*, inside 8.6 kpc, tends to run perpendicular to the galactic plane, and individual features tend to persist with velocity over several frames. These vertical structures are wiggly, and look very much like worms crawling out of the galactic plane.

We believe that these "worms" are parts of incomplete shells. In the solar neighborhood there is a similar looking structure: the H I gas surrounding the North Polar Star—the "HINPS" (see review by Heiles *et al.* 1980). The HINPS is best seen on the photographs of Colomb, Pöppel, and Heiles (1980). The brightest part of the HINPS is a vertical pillar of gas, and, if viewed from afar with relatively poor angular resolution and at low sensitivity, it would look very much like a "worm." By analogy with the NPS, at least some of the H I worms should have radio continuum emission running alongside them, but not exactly superposed. Unfortunately, however, it is probably impossible to detect such radio continuum "worms" because of confusion with foreground and background radio continuum emission—just as the H I worms would be undetectable without being able to use velocity to isolate the H I at one or two particular distances.

The structure of the worms suggests that the tops of their shells are usually open. Shells should be filled with very hot gas. A shell that is open at the top provides an escape hatch into the halo for this hot gas. There seems to be a large number of such structures in the inner galaxy. They should be prolific sources of hot gas for the galactic halo.

V. WHAT PRODUCES THESE H I STRUCTURES?

a) Brief Summary of the Observational Data

Historically, the first observation of an H I shell was made by Menon (1958), who found an expanding shell in the Orion region. Katgert (1969) discovered the shell GS 061−0+51 (of Heiles 1979), which is unrelated to any other known object. Velden and Hirth (1982) found a shell centered near $(l, b) = (130°, 22°.5)$, which is quite possibly associated with a pulsar. Stacy and Jackson (1982) found six shells in the Puppis window of the Milky Way. Lockman and Ganzel (1983) found an unusual "bipolar flow" of H I near $(l, b) = (207, 1)$, which might possibly be an incomplete expanding shell. The Sun itself is located within an expanding H I shell (Hughes and Routledge 1972; Lindblad *et al.* 1973; Olano and Pöppel 1981). Other shells, visible in optical emission lines, have been summarized by Brand and Zealey (1975). The aforementioned shells, plus those cataloged in Paper I, in Hu (1981), and in the present study, number more than 150.

There is no one-to-one relationship of H I shells with supernova remnants. A search in Paper I for shells associated with 16 radio-emitting supernovae found only five possible associations with faint H I features not prominent enough to have been independently recognized as shells. However, shells associated with several supernova remnants have been discovered: HB 21 (Assousa and Erkes 1973); IC 443 (Giovanelli and Haynes 1979); G261.9+5.5 (Colomb and Dubner 1980); the Lupus Loop (Colomb and Dubner 1982); CTB 1 (Landecker, Roger, and Derdney 1982); and W44 (Knapp and

Kerr 1974). Searches for H I shells associated with the Cygnus Loop (DeNoyer 1975; Giovanelli and Haynes 1979) were negative.

There is no one-to-one relationship of shells with young star clusters and associations. Many of the shells listed here and in Paper I are not related to known stellar associations on clusters. Nevertheless, there are some definite associations of shells and stellar associations and clusters: one with Per OB2 (Sancisi 1974), one with Sco OB2 (Sancisi 1974), and one or two with Cep OB3 (Read 1980). As discussed above, the shell associated with radio loop I is probably produced by stars in the Sco/Oph associations. Six shells in Paper I are associated with stellar associations and clusters, and possibly some other weak, almost unrecognizable shells might be associated with other clusters. However, nine clusters have no hint of an associated shell. And a search for shell around 13 OB associations yielded only two shells, around Orion and Carina (Cowie *et al.* 1981).

Shells and supershells have also been observed in external galaxies, as summarized in Paper I. More recently, a 700 pc diameter in NGC 55 has been discovered by Graham and Lawrie (1982). In the LMC, Goudis and Meaburn (1978) and Meaburn (1980) have isolated 85 "giant" shells (20–260 pc diameter) and six "supergiant" shells (~ 1 kpc diameter) from specially processed optical plates. In addition, Brinks (1981, 1983) has mapped the H I in M31 with the WSRT and found a plethora of H I holes and shells. The study of shells in external galaxies probably offers the best way to understand their origins.

b) Interpretive Discussion

The summary of the above section is that there is no unique relationship between shells and any other type of astronomical object. Some shells are definitely associated with supernovae and some with young stellar clusters—but not all supernovae and clusters have shells, and most shells are not associated with any common astronomical objects. Although it is conceivable that old shells are associated with stellar clusters that are now too old to be recognizable, another explanation for the origin of shells and supershells seems to be required.

In addition, there are shells or shell-like objects that do not fit well with an origin involving the release of energy by stars. Some of these have very large energies, so large that they seem incommensurate with the level of star formation, particularly in the outer galaxy. And some shells or shell-like structures, discussed in § III, have large systemic velocities; it would seem that an external source of momentum is required.

One other explanation involves the collision of HV clouds with the galactic disk. We discuss these two possibilities in light of the observational data.

i) *Stellar Winds and Supernova*

For those shells that are associated with supernova or star clusters, the source of energy is clearly the stars. In those cases that are well studied, the energy required is consistent with that available from the stars. This is the case for the LMC (Braunsforth and Feitzinger 1983), even for the "giant" shells (Meaburn 1980; Blades, Elliot, and Meaburn 1980; de Boer and Nash 1982) that require energies of more than 10^{53} ergs. However, if stars are to provide the energy for the "supergiant" shells in the LMC, the requirements are more severe: for LMC2, the current rate of star formation must have existed for the past 10^7 yr (Caulet *et al.* 1982)—and whether this can occur for all of the supergiant shells is a matter of opinion (see Meaburn 1980).

Shells in our own Galaxy are more difficult to analyze because of distance ambiguities, but the required energies seem to be available for the NPS region (see, e.g., Cox and Anderson 1982) and the X-ray emitting "Cygnus superbubble" (Cash *et al.* 1980; Higdon 1981). The former of these is a modest H I supershell with a radius of only 100 pc, and could even be the result of the dynamical evolution of the H II region formed by the stars inside, as discussed theoretically by Tenorio-Tagle *et al.* (1982) and Beltrametti, Tenorio-Tagle, and Yorke (1982). The latter is probably not an H I shell at all (Higdon 1981).

It is natural to hypothesize that all shells, even the supershells, are caused by stars and supernovae (Bruhweiler *et al.* 1980). However, this hypothesis meets with difficulty because of the energy requirements. As specific examples, five supershells[1] in Paper I are estimated to have kinetic energies of more than 10^{53} ergs, with radii ranging up to 1.3 kpc and expansion velocities up to 24 km s^{-1}. Bruhweiler *et al.*'s shell models have a radius of 520 pc (parallel to the plane) and an expansion velocity of 5 km s^{-1}, at the end of the "second supernova burst phase" of a "typical" OB association with 28 stars B0 and earlier (equivalent to the Sco OB1 association), expanding in an ambient density of 0.1 cm^{-3}. In comparison with the largest observed supershells, such a shell is puny; it has swept up less than 10% of the mass, and expands at one-fourth the velocity of the largest observed supershells. If the concept of energy input from stars is to explain these largest supershells, the association or cluster must be ~ 100 times larger than the Sco OB1 association. Such star-formation activity might possibly occur in the LMC, but there is no independent evidence that it occurs in our own Galaxy—particularly outside the solar circle, where most supershells reside and where star formation activity is presumably quite moderate.

Bruhweiler *et al.* assumed the interstellar medium to be the homogeneous, classical "intercloud medium" of Field, Goldsmith, and Habing (1969). As an alternative, the theory of the interstellar medium by McKee and Ostriker (1977) pictures most of the volume occupied by the "HIM"—a very rarefied, hot component of the interstellar gas. Owing to the low density of this gas, the release of a given amount of energy results in a larger shell than it does for the classical intercloud medium. The numerical models of Chevalier (1974) show that, for a given energy and expansion velocity, the shell radius is proportional to $n_0^{0.36}$, where n_0 is the ambient density. Thus, a smaller ambient density can easily result in shells with the observed radius and expansion velocity. However, such shells do not contain the observed amount of mass—or in other words, they do not exhibit the observed kinetic energy. While it is true that the observed masses are quite uncertain (Paper

[1]Parameters for two shells in Table 1 of Paper I are given incorrectly. For GS 123+07−127 and GS 139−03−69, the linear radii, masses, and energies in Paper I are too high by factors of 2, 4, and 4, respectively.

I), they should not be so uncertain as to reduce the derived kinetic energies by large factors of order 10. Thus, in the final analysis, the observed kinetic energies can be obtained only by injecting more energy into the interstellar medium than is available from a typical star cluster, or by injecting it more efficiently.

Elmegreen and Chiang (1982) have discussed a new source of energy for a preexisting, large shell: the radiation pressure from ordinary stars enclosed within the shell. Unfortunately, their mechanism requires such a large preexisting shell that it is unlikely to be important until a shell has already reached supershell status. The radiation pressure inside a shell, the interior of which has been swept clear of dust, is larger than that outside the shell, where dust absorbs light from distant stars. If a shell encompasses a sufficiently large number of ordinary stars, i.e., has a large enough radius, then the radiation pressure difference across the shell boundary dominates all other forces and the shell expands with an ever-increasing velocity—it "runs away." This mechanism is only effective for shells having larger than critical values of radius and expansion velocity. These critical values depend on the ratio $R =$ (starlight radiation density)/(pressure of interstellar medium). Before this mechanism can be effective, and produce runaway expansion, a preexisting shell 1 kpc in radius must be expanding faster than 10 km s^{-1} and one 600 pc in radius must be expanding faster than 50 km s^{-1} (our assumed value for R is that given by Elmegreen and Chiang for the solar vicinity, and that for the effective sound speed in the interstellar medium is 3.4 km s^{-1}, which is consistent with the other assumed interstellar parameters). These requirements are very severe and require the previous injection of a large amount of energy from some other source. The mechanism can be effective in producing supershells from smaller ones only if the ratio R is significantly larger than that assumed, by a factor of 10 or so. Elmegreen and Chiang (1982) also consider the mechanism in the absence of resistance to expansion by external pressure, which might occur if there is a large number of diffuse clouds, imbedded in a tenuous intercloud medium, that are swept up into a shell. The mechanism is effective in this case for any shell with radius larger than 300 pc, no matter what its expansion velocity, again in the solar vicinity. However, if a shell is free to expand without resistance to external pressure, other calculations of shell dynamics—such as that of Bruhweiler *et al.* (1980)—need to be modified, and will also provide larger radii. The full implications of this possibility are beyond the scope of other theoretical work known to this author.

ii) *Collision of High-Velocity Clouds with the Galactic Disk*

For the most energetic supershells and some shell-like objects with gas spanning a velocity range of 100 km s^{-1} or more and having large systemic velocities, another completely independent origin might be at work. The most prominent alternative is collisions of HV clouds with the galactic disk (Tenorio-Tagle 1980, 1981). An infalling cloud transfers a large fraction of its kinetic energy to the ambient gas in the disk; energy requirements are met fairly easily for clouds similar to those observed.

There are three arguments that favor this mechanism. The first is based on statistics and energy requirements. In the LMC, the histogram of shell sizes is separated into two distinct ranges—the "giant" and the "supergiant" shells (Goudis and Meaburn 1978; Meaburn 1980). And in our own Galaxy, Paper I postulated the existence of "supershells," as distinct from "shells," because of the extraordinarily large energies involved, although there was no obvious bifurcation of the histogram of shell sizes.

The second argument concerns the apparent association of some supershells with HV gas. The discussion of observational data in § III mentioned three possible shells or supershells that are associated with HV gas—associated to the extent that it is even possible to consider the HV gas as part of the shell, if enough liberality is allowed in the interpretation. These are GS 120−30−8, GS 155+38−58, and GS 174+02−64. All of these shell-like objects cover large velocity ranges and seem to have significant systemic velocities, and thus net momenta with respect to ambient gas. Momentum transfer from infalling gas is a natural source for this momentum. The last of these objects, the "anticenter shell," is the best example of the collision mechanism because of the correlations between high and low velocity gas on small angular scales reviewed in § III.

Finally, as noted in Paper I, only one hemisphere of most of the shells that are still expanding is visible—this is a prediction of the theory (Tenorio-Tagle 1980)! In fact, every one of the most energetic expanding supershells in Paper I has only one hemisphere visible.

VI. SUMMARY

1. We have presented photographic representations of the combination of two H I surveys so as to eliminate the artificial boundaries at $|b| = 10°$. We have also presented photographic representations having more contrast for some velocities to exhibit weaker H I features.

2. We have used them to prepare a new list of H I shells and supershells in Table 1. The recognition and measurement of a shell is a difficult subjective process, and the entries in Table 1 are so incomplete and uncertain that Table 1 is unsuitable for statistical purposes.

3. We have discussed in some detail three shell-like objects —GS 120−30−9, GS 155+38−58, and GS 174+02−64—that seem to be associated with very high velocity gas. The former two of these overlap radio continuum loops II and III. Possible causal connections among low, intermediate, and high velocity gas are discussed. There is no compelling evidence for a direct association, but the apparent superposition of H I over velocity ranges spanning 100 km s^{-1} or more is strongly suggestive. These objects may have large systemic velocities.

4. We summarize the properties of the most prominent shell in the sky—GS 331+14−15. This shell is associated with radio loop I (the North Polar Spur) and soft X-ray emission. It is expanding at ~ 25 km s^{-1} and is ~ 120 pc in diameter. The shell structures in this region can be explained by successive energy inputs from supernovae, stellar winds, and H II regions from the star clusters located inside the shells.

5. We review the observational data on shells, supershells, and shell-like objects. There is no unique relationship between shells and any other type of astronomical object. Only some shells are definitely associated with supernovae or star clusters. Most supernovae and clusters are not associated with

shells. Most shells do not seem to be associated with any common astronomical object.

6. Stellar winds and supernovae in stellar associations are adequate energy sources for many shells.

7. Stellar winds and supernovae in stellar associations are not adequate energy sources for the largest H I supershells, unless the star clusters are very much larger than usual. Presumably, this is not the case, particularly outside the solar circle where supershells tend to be found.

8. The collision of high-velocity clouds with the galactic disk is a mechanism for injecting momentum and large amounts of energy into the interstellar medium. Notably, this mechanism is consistent with three aspects of the data. These are the existence of some very large and energetic shells or shell-like objects; the observed association, in some cases, of low and high velocity gas; and the preponderance of expanding shells with only one observable hemisphere. Production by infalling gas can account for many of the observational details. The infalling gas may be fragments of the Magellanic stream.

9. In the inner galaxy for radii smaller than ~ 8.6 kpc, spatial filtering applied to H I survey data reveals "worms" of gas—wiggly filaments that tend to run perpendicular to the galactic plane. These are really shells with open tops and should be prolific sources of hot gas for the galactic halo.

It is a pleasure to acknowledge discussions with F. J. Lockman and M. Elitzur, and support from the National Science Foundation.

REFERENCES

Allen, R. J., and Goss, W. M. 1979, *Astr. Ap. Suppl.*, **36**, 135.
Allen, R. J., Goss, W. M., and van Woerden, H. 1973, *Astr. Ap.*, **29**, 447.
Assousa, G. E., and Erkes, J. W. 1973, *A.J.*, **38**, 885.
Bates, B., Brom-Kern, W., Gieretta, D. L., and Keenan, F. P. 1983, *Astr. Ap.*, **122**, 64.
Beltrametti, M., Tenorio-Tagle, G., and Yorke, H. W. 1982, *Astr. Ap.*, **112**, 1.
Berkhuijsen, E. M., Haslam, C. G. T., and Salter, C. J. 1971, *Astr. Ap.*, **14**, 252.
Blades, J. C., Elliot, K. H., and Meaburn, J. 1980, *M.N.R.A.S.*, **192**, 101.
Brand, P. W. J. L., and Zealey, W. J. 1975, *A.J.*, **38**, 363.
Braunsforth, E., and Feitzinger, J. V. 1983, *Astr. Ap.*, **127**, 113.
Brinks, E. 1981, *Astr. Ap.*, **95**, L1.
_____. 1983, in *The Leiden Southern Hemisphere Workshop*, ed. F. Israel (Dordrecht: Reidel), in press.
Bruhweiler, F. C., Gull, T. R., Kofatos, M., and Sofia, S. 1980, *Ap. J. (Letters)*, **238**, L27.
Burton, W. B., and Moore, R. L. 1979, *A.J.*, **81**, 189.
Castor, J., McCray, R., and Weaver, R. 1977, *Ap. J. (Letters)*, **200**, L107.
Caulet, A., Deharveng, L., Georgelin, Y. M., and Georgelin, Y. P. 1982, *Astr. Ap.*, **110**, 185.
Chevalier, R. A. 1974, *Ap. J.*, **188**, 501.
Cohen, R. J. 1981, *M.N.R.A.S.*, **196**, 835.
Cash, W., Charles, P., Bowyer, S., Walter, F., Garmire, G., and Riegler, G. 1980, *Ap. J. (Letters)*, **238**, L71.
Colomb, F. R., and Dubner, G. 1980, *Astr. Ap.* **82**, 244.
_____. 1982, *Astr. Ap.*, **112**, 141.
Colomb, F. R., Pöppel, W. G. L., and Heiles, C. 1980, *Astr. Ap. Suppl.*, **40**, 47.
Cowie, L. L., Hu, E. M., Taylor, W., and York, D. G. 1981, *Ap. J. (Letters)*, **250**, L25.
Cox, D. P., and Anderson, P. R. 1982, *Ap. J.*, **253**, 268.
Crutcher, R. M. 1982, *Ap. J.*, **254**, 82.
Davelaar, J., Bleeker, J. A. M., and Deerenberg, A. J. M. 1980, *Astr. Ap.*, **92**, 231.
Davies, R. D. 1972, *M.N.R.A.S.*, **160**, 381.
de Boer, K. S., and Nash, A. G. 1982, *Ap. J.*, **255**, 447.
DeNoyer, L. K. 1975, *Ap. J.*, **196**, 479.
DeNoyer, L. K., Button, L., Chaffin, D., and Nieznanski, J. 1977, *Ap.J.*, **213**, 379.
Dieter, N. H. 1971, *Astr. Ap.*, **12**, 59.
Elmegreen, B. G., and Chiang, W. 1982, *Ap.J.*, **253**, 666.
Field, G. B., Goldsmith, D. W., and Habing, H. 1969, *Ap. J. (Letters)*, **155**, L49.
Giovanelli, R. 1980*a*, *A.J.*, **85**, 1155.
_____. 1980*b*, *Ap.J.*, **238**, 554.
Giovanelli, R., and Haynes, M. 1979, *Ap.J.*, **230**, 404.
Goudis, C., and Meaburn, J. 1978, *Astr. Ap. (Letters)*, **68**, 189.
Graham, J. A., and Lawrie, D. G. 1982, *Ap. J. (Letters)*, **253**, L73.
Heiles, C. 1974, *Ap. J. (Letters)*, **193**, L31.
_____. 1976, *Ap. J. (Letters)*, **208**, L137.
_____. 1979, *Ap.J.*, **229**, 533.
_____. 1983*a*, in *Kinematics, Dynamics, and Structure of the Milky Way*, ed. W. L. H. Shuter (Dordrecht: Reidel), p. 105.
_____. 1983*b*, in *The Leiden Southern Hemisphere Workshop*, ed. F. Israel, (Dordrecht: Reidel), in press.
Heiles, C. 1983*c*, *Nuovo Cimento*, in press.
Heiles, C. Chu, Y-H., Reynolds, R. J., Yegingil, I., and Troland, T. H. 1980, *Ap. J.*, **242**, 533.
Heiles, C., and Habing, H. J. 1974, *Astr. Ap. Suppl.*, **14**, 1.
Higdon, J. C. 1981, *Ap.J.*, **244**, 88.
Hu, E. 1981, *Ap.J.*, **248**, 119.
Hughes, V. A., and Routledge, D. 1972, *A.J.*, **77**, 210.
Iwan, DeAnn. 1980, *Ap.J.*, **239**, 316.
Katgert, P. 1969, *Astr. Ap.*, **1**, 54.
Kepner, M. 1970, *Astr. Ap.*, **5**, 444.
Knapp, G. R., and Kerr, F. J. 1974, *Astr. Ap.*, **33**, 463.
Landecker, T. L., Roger, R. S., and Derdney, P. E. 1982, *A.J.*, **87**, 1397.
Lindblad, P. O., Grape, K., Sandquist, A., and Scheler, J. 1973, *Astr. Ap.*, **24**, 309.
Lockman, F. J., and Ganzel, B. L. 1983, *Ap.J.*, **268**, 117.
McCammon, D., Burrows, D. N., Sanders, W. T., and Kraushaar, W. L. 1983, *Ap.J.*, **269**, 107.
McKee, C. F., and Ostriker, J. P. 1977, *Ap.J.*, **211**, 135.
Meaburn, J. 1980, *M.N.R.A.S.*, **192**, 365.
Menon, T. K. 1958, *Ap. J.*, **127**, 28.
Mirabel, I. F. 1982, *Ap.J.*, **256**, 112.
Moore, R. L., and Burton, W. B. 1979, in *IAU Symposium 84, The Large-Scale Characteristics of the Galaxy*, ed. W. B. Burton (Dordrecht: Reidel), p. 535.
Naranan, S., Schulman, S., Friedman, H., and Fritz, G. 1976, *Ap.J.*, **208**, 718.
Olano, C. A. 1982, *Astr. Ap.*, **112**, 195.
Olano, C. A., and Pöppel, W. G. L. 1981, *Astr. Ap.*, **94**, 151.
Read, P. 1980, *M.N.R.A.S.*, **193**, 487.
Reynolds, R. J., and Ogden, P. M. 1979, *Ap.J.*, **229**, 942.
Sancisi, R. 1974, in *IAU Symposium 60, Galactic Radio Astronomy*, ed. F. J. Kerr and S. C. Simonson (Dordrecht: Reidel), p. 573.
Simonson, S. C. 1975, *Ap. J. (Letters)*, **201**, L103.
Stacy, J. G., and Jackson, P. D. 1982, *Astr. Ap.*, **50**, 377.
Stark, A. A., Heiles, C., Bally, J., and Linke, R. 1983, in preparation.
Tenorio-Tagle, G. 1980, *Astr. Ap.*, **88**, 61.
_____. 1981, *Astr. Ap.*, **94**, 338.
Tenorio-Tagle, G., Beltrametti, M., Bodenheimer, P., and Yorke, H. W. 1982, *Astr. Ap.*, **112**, 104.
Treffers, R. R., and Chu, Y-H. 1982, *Ap.J.*, **254**, 569.
Troland, T. H., and Heiles, C. 1982, *Ap. J. (Letters)*, **260**, L19.
Velden, L., and Hirth, W. 1982, *Astr. Ap.*, **113**, 340.
Verschuur, G. L. 1971, *Astr. J.*, **76**, 317.
_____. 1973, *Astr. Ap.*, **22**, 139.
_____. 1975, *Ann. Rev. Astr. Ap.*, **13**, 257.
Watanabe, T. 1982, *Astr. Ap.*, **111**, 333.
Weaver, H. F. 1974, in *IAU Symposium 60, Galactic Radio Astronomy*, ed. F. J. Kerr and S. C. Simonson (Dordrecht: Reidel), p. 573.
_____. 1979, in *IAU Symposium 84, The Large-Scale Characteristics of the Galaxy*, ed. W. B. Burton (Dordrecht: Reidel), p. 295.
Weaver, H. F., and Williams, D. R. 1973, *Astr. Ap. Suppl.*, **8**, 1.
Wesselius, P. R., and Fejes, I. 1973, *Astr. Ap.*, **24**, 15.
Westerlund, B. E., and Mathewson, D. S. 1966, *M.N.R.A.S.*, **131**, 371.

CARL HEILES: Astronomy Department, University of California, Berkeley, CA 94720